THE TORQUE AND ANGULAR VELOCITY INDUCED BY THE GEOMAGNETIC FIELD ON A SPINNING CONDUCTING SATELLITE

by

G. Louis Smith

Thesis submitted to the Graduate Faculty of the

Virginia Polytechnic Institute

in candidacy for the degree of

MASTER OF SCIENCE

in

AEROSPACE ENGINEERING

May 1963

Blacksburg, Virginia

II. TABLE OF CONTENTS

III. LIST OF FIGURES

FIGURE PAGE

IV. INTRODUCTION

One source of torques on near-earth satellites is due to the interaction of the earth's magnetic eddy currents induced in the electrically conducting parts of a spinning satellite. The geomagnetic field induces eddy currents within the rotating conducting shell; these in turn produce a torque. Estimates of this torque are given for various satellites in references 1 to 4. These estimates consider only the effect of the component of torque which reduces the rotation. It is demonstrated in reference 5 that there also exists a component of torque normal to the spin vector; this will tend to change the direction of the spin vector.

At present, the literature on this subject deals primarily with spheres and spherical shells (see refs. 5 and 6).

As a satellite travels in its orbit about the earth, the magnetic field which the satellite encounters will vary considerably. In reference 7, equations are presented, and an IBM-704 computer program is described, for numerically evaluating the decay or damping of the spin motion due to eddy-current torques. However, only the torque component parallel to the spin axis, which damps the spin, is considered in reference 7.

It is seen that the problem of determining the effect of torques due to magnetically induced eddy currents is of two parts: first, the calculation or measurement of the torque, on the satellite, due to a known magnetic field; and second, the calculation of the torques and their effect on the angular motions of the satellite while the vehicle is in orbit around the earth.

This thesis presents studies on both parts of this problem.

First, the cases for a cylinder rotating about its centerline, and about an axis normal to its centerline are studied. The latter case is of interest because many cylindrical satellites tumble after injection into orbit. Next, thin cones and frustums of cones are investigated; equations are derived for the induced currents within the shell, from which the torques follow. A method is described for extending these results to a series of frustums joined together. This method leads to a solution for a general body of revolution. In each case studied, equations are derived for the current density throughout the body and for the total resultant torque.

Expressions are derived and presented for the average torques due to eddy currents while the satellite is in orbit around the earth; and, the resulting time history of the spinning motion is studied.

Because of the rather large number of symbols necessary and the natural division of the problem into two parts, the analysis is presented in this manner; each part has its separate list of symbols.

V. LIST OF SYMBOLS

A. Symbols for Part I of analysis

C	curve of integration
c	velocity of light
$\overline{E}$	electric field intensity vector
E (with subscript)	component of $\overline{E}$
$\overline{e}_1$, $\overline{e}_2$, $\overline{e}_3$	unit vectors along ξ, η, and ζ axes
$\overline{F}$	force per unit volume
$\overline{H}$	magnetic field intensity vector
h	magnitude of $\overline{H}$
$\overline{i}$, $\overline{j}$, $\overline{k}$	unit vectors along X, Y, and Z axes
$\overline{J}$	current density vector
J (with subscript)	component of $\overline{J}$
$J_n(\ )$	Bessel function of first kind, of order n
k_n, k_{nm}	eigenvalues in thick-wall cylinder solution
$\overline{L}$	torque vector
l	length of cylinder
P(x)	function defined by equation (36)
$\overline{r}$	radius vector
r	radius (cylindrical coordinate)
t	time
$\overline{u}$ (with subscript)	unit vector, in direction indicated
w	transformation variable, defined by equation (71)
x, y, z	distance along coordinate axes X, Y, and Z
$Y_n(\ )$	Bessel function of second kind, of order n

$Z_n(\ )$	cylinder function of order n, $E_{nr}J_n(\ ) + F_{nn}Y_n(\ )$
a_n	quantities defined by equation (40)
β_n	quantities defined by equation (46)
θ	angle from X-axis in X, Y plane (cylindrical and spherical coordinate)
λ	angle between Z-axis and $\overline{H}$
μ	angle defined in figure 10 for tumbling-cylinder analysis
ν	polar angle in plane, used in cone analysis
ξ, η, ζ	coordinate axes used in analysis of tumbling cylinder (see fig. 10)
ρ	distance along cone from vertex to point (spherical coordinate)
σ	electrical conductivity
τ	thickness of thin wall
Φ	harmonic function; for example, equation (13)
ϕ	cone half-angle (fig. 11)
$\underline{\psi}$	vector potential of $\overline{J}$
Ψ	stream function
$\overline{\omega}$	spin vector
ω	spin rate

Subscripts:

a, b	quantity evaluated at end a or end b
i	inside
o	outside
av	average

B. Symbols for Part II of analysis

A	square matrix, defined by equation (14)
A'	square matrix, defined in equation (4)
c_i	coefficient of eigenvector
$B(i_I)$	square matrix, defined by equation (34)
$B(i_I, \mu)$	square matrix, defined by equation (32)
b_{ij}	elements of $B(i_I)$
e_i	eigenvector
e	2.718...., Napierian Base
$\overline{H}$	magnetic field vector
H_i	component of magnetic field vector
I	identity matrix
I_{max}	maximum moment of inertia of satellite
$\overline{i}, \overline{j}, \overline{k}$	unit vectors
K	interaction constant (see eq. (1))
$\overline{M}$	torque
m	earth's gravitation constant
P	period of satellite orbit
p	semi-latus rectum of orbit
r	geocentric radius
s	geomagnetic dipole strength
T	transformation matrix (with subscript)
t	time
X	coordinate vector
x, y, z	Cartesian coordinates
$\alpha, \beta, \gamma, \delta$	elements of A matrix

e	eccentricity
ζ	tilt angle of dipole
θ	true anomaly
η	argument of perigee
i	orbital inclination
λ	eigenvalue of A matrix
μ	angle of earth rotation
ν	angle from x_m to x_g
π	3.14159...
τ	time (nondimensional)
χ	angle from y-axis to e_2
ϕ	satellite longitude
ψ	satellite colatitude
$\bar{\omega}$	spin vector
ω	spin rate

Subscripts:

$(\ )_E$	earth fixed reference
$(\ )_I$	space fixed, or inertial, reference
$(\ )_M$	geomagnetic reference
$(\ )_0$	initial condition

VI. ANALYSIS, PART I

A. GOVERNING EQUATIONS AND BOUNDARY CONDITIONS

In order to formulate the problem mathematically, it is necessary first to list the equations and the boundary conditions to be used. Maxwell's equations describe the magnetic and electric fields inside and outside the cylinder (see refs. 4 and 6). The analysis is restricted to nonferromagnetic metals so that, in Gaussian units, the permittivity and permeability are near unity. Also, for spin rates reasonable for most satellites, the magnetic field due to the induced eddy currents is small compared with the primary field; therefore, the unperturbed magnetic field can be used in the electric field equations. This approximation is justified in reference 4. Also, for spin rates of the magnitude applicable to satellites, the charge density within a conductor will be negligible. Thus, as is shown in reference 4, the electric field equations are

$$\nabla \times \overline{E} = -c^{-1} \frac{\partial \overline{H}}{\partial t} \tag{1}$$

$$\nabla \cdot \overline{E} = 0 \tag{2}$$

In stationary axes, the electric field can be written (ref. 4) as:

$$\overline{E} = \nabla \Phi + c^{-1}(\overline{\omega} \times \overline{r}) \times \overline{H} \tag{3}$$

where $\nabla^2 \Phi = 0$, and Φ, the potential of the electric field, is determined by the boundary conditions. The term $c^{-1}(\overline{\omega} \times \overline{r}) \times \overline{H}$ is the induced electric field. The current follows immediately from

$$\overline{J} = \sigma \overline{E} \tag{4}$$

The force per unit volume is then

$$\overline{F} = c^{-1} \overline{J} \times \overline{H} \tag{5}$$

and the torque is calculated by integrating the differential torque

$$d\overline{L} = \overline{r} \times d\overline{F} \tag{6}$$

The only boundary condition is that the component of current (or electric field) normal to the surface vanish at the surface. This condition, together with the induced field, is sufficient to determine Φ and $\nabla\Phi$ completely.

Equation (3) is well suited for calculating the electric field in symmetrically spinning cylinders, inasmuch as the boundary condition can be readily applied in this case to determine Φ; it will be used in the study of both symmetrically spinning thin-wall and thick-wall cylinders. However, in calculating the electric field in thin-wall tumbling cylinders and spinning cones, equation (3) is not so well suited, and it becomes convenient to use a stream function to solve equations (1) and (2) simultaneously.

B. SYMMETRICALLY SPINNING CYLINDER

For the symmetrically spinning cylinder, an approximate solution is first obtained for the thin-wall shells. The solution for the thick-wall cylinder is then derived, and a comparison is made of the two solutions.

To study the case of a symmetrically spinning open-ended cylinder, Cartesian and cylindrical coordinate systems are first set up as shown in figure 1. The Z-axis is set up along the center line of the cylinder, and the X-axis is defined in such a way that $\overline{H}$ lies in the X,Z plane and forms an angle λ with the Z-axis. The quantities $\overline{H}$, $\overline{r}$, and $\overline{\omega}$ can then be written as

$$\overline{H} = h(\overline{i} \sin \lambda + \overline{k} \cos \lambda)$$

$$= h(\overline{u}_r \sin \lambda \cos \theta - \overline{u}_\theta \sin \lambda \sin \theta + \overline{u}_z \cos \lambda) \tag{7}$$

$$\overline{r} = \overline{u}_r r + \overline{u}_z z \tag{8}$$

$$\overline{\omega} = \overline{u}_z \omega \tag{9}$$

Equation (3) thus becomes

$$\overline{E} = \nabla\Phi + c^{-1}h\omega r(\overline{u}_r \cos \lambda - \overline{u}_z \sin \lambda \cos \theta) \tag{10}$$

The boundary conditions may then be written as

$$E_z\left[r, \theta, \pm \frac{l}{2}\right] = 0 \tag{11}$$

$$E_r(r_i, \theta, z) = E_r(r_o, \theta, z) = 0 \tag{12}$$

1. Thin-Wall Case

For a thin-wall open-ended cylindrical shell, the radial component of flow will be negligible by comparison with the circumferential and longitudinal components, J_θ and J_z, respectively, and J_θ and J_z will not vary significantly between $r = r_i$ and $r = r_o$. The problem, therefore, can be considered to be primarily dependent on θ and z.

Since the cylinder can then be cut along an element and developed onto a plane, the problem may be treated as two-dimensional, with $r\theta$ as the abscissa and z as the ordinate, where r is taken to be the "average" radius. Only a strip of the plane one period in width need be considered. A potential field $\nabla\Phi$ is now superimposed on the field and adjusted to make the longitudinal components of the total field vanish at the boundaries of the region corresponding to the open ends of the cylinder. The potential then is (ref. 6)

$$\Phi = \sum_{n=0}^{\infty} (A_n \sin n\theta + B_n \cos n\theta) \left(C_n \sinh \frac{nz}{r} + D_n \cosh \frac{nz}{r}\right) \qquad (13)$$

Equation (10) thus becomes

$$\overline{E} = -u_z c^{-1} h \omega r \sin \lambda \cos \theta + \overline{u}_z \sum_{n=0}^{\infty} (A_n \sin n\theta + B_n \cos n\theta) \left(C_n \cosh \frac{nz}{r} + D_n \sinh \frac{nz}{r}\right) \frac{n}{r} + \frac{u_\theta}{r} \sum_{n=0}^{\infty} n(A_n \cos n\theta - B_n \sin n\theta) \left(C_n \sinh \frac{nz}{r} + D_n \cosh \frac{nz}{r}\right) \qquad (14)$$

The radial components have been dropped in equation (14) for this thin-wall case; thus, equations (12) are satisfied automatically. In order to satisfy the boundary condition (11), it is necessary that the first term of equation (14) cancel the first summation at $z = \pm \frac{l}{2}$, for all values of θ. This requires that all the coefficients be zero except B_1 and C_1, as only the cos θ term of the harmonic does not vanish identically. Then

$$0 = -c^{-1}h\omega r \sin\lambda \cos\theta + \frac{B_1C_1}{r}\cos\theta \cosh\frac{l}{2r}$$

from which

$$B_1C_1 = \frac{c^{-1}h\omega r^2 \sin\lambda}{\cosh\frac{l}{2r}} \tag{15}$$

Substituting equation (15) into equation (13) gives the potential as

$$\Phi(\theta,z) = c^{-1}h\omega r^2 \sin\lambda \cos\theta \frac{\sinh\frac{z}{r}}{\cosh\frac{l}{2r}} \tag{16}$$

The electric field is then

$$\overline{E}(\theta,z) = -\overline{u}_z c^{-1}h\omega r \sin\lambda \cos\theta \left(1 - \frac{\cosh\frac{z}{r}}{\cosh\frac{l}{2r}}\right)$$

$$- u_\theta c^{-1}h\omega r \sin\lambda \sin\theta \frac{\sinh\frac{z}{r}}{\cosh\frac{l}{2r}} \tag{17}$$

The electric field having been determined, the current follows immediately by equation (4). The torque is then calculated by

$$\overline{L} = c^{-1}\int_V \overline{r} \times (\overline{J} \times \overline{H})dV \tag{18}$$

where V is volume. Equations (7), (8), and (17) are substituted into the integrand of equation (18). The resulting vector expression in terms of $\overline{u}_r$, $\overline{u}_\theta$, and $\overline{u}_z$ is then referred to the X,Y,Z system in terms of $\overline{i}$, $\overline{j}$, and $\overline{k}$. The result is then integrated over the surface of the cylinder. (Because of the thin-wall approximations, the integration

with respect to r is replaced by simply multiplying by the thickness τ.) The final result is

$$\bar{L} = \pi\sigma c^{-2}h^{2}\omega \sin\lambda\, r^{3}l\tau\left(1 - \frac{2r}{l}\tanh\frac{l}{2r}\right)(\bar{i}\cos\lambda - \bar{k}\sin\lambda) \qquad (19)$$

The factor $1 - \frac{2r}{l}\tanh\frac{l}{2r}$, which is the torque per unit length normalized with respect to the torque per unit length of a similar cylindrical shell of infinite length, is plotted as a function of fineness ratio in figure 2. It is seen from this figure that the torque per unit length increases rapidly with fineness ratio up to a ratio of approximately 5, after which the torque per unit length is a weak function of fineness ratio. The torque, similarly normalized, is shown in figure 3.

The conventional stream function ψ, describing the current paths within the cylindrical shell, is defined by

$$\left.\begin{aligned}\frac{\partial\psi}{r\,\partial\theta} &= J_z = \sigma E_z\\ \frac{\partial\psi}{\partial z} &= -J_\theta = -\sigma E_\theta\end{aligned}\right\} \qquad (20)$$

Dimensionally, this definition corresponds to a unit thickness. Then by equation (17)

$$\psi(\theta,z) = -\sigma c^{-1}h^{\omega}r^{2}\sin\lambda\sin\theta\left(1 - \frac{\cosh\frac{z}{r}}{\cosh\frac{l}{2r}}\right) \qquad (21)$$

The current paths, or streamlines, are given by lines of constant ψ and are shown in figures 4(a), 4(b), and 4(c) for fineness ratios of 2, 4, and 8, respectively. The mapping for $\pi \leq \theta \leq 2\pi$ will be identical

to that shown for $0 \leq \theta \leq \pi$. The values of ψ have been normalized by dividing by the maximum value. The direction of the flow depends, of course, on the relative direction of the spin vector and the applied magnetic field vector and thus is not indicated. Comparison of these figures shows physically why the torque per unit length varies as it does with fineness ratio. As the fineness ratio is increased, the current paths become more nearly straight and parallel, except near the ends; thus, in the limiting case of an infinite cylinder, the streamlines are parallel.

In the preceding analysis the problem of the torque and eddy currents produced by a conducting cylindrical shell spinning in a magnetic field has been studied on the basis of thin-wall approximations. Exact solutions to the problem for a thick-wall cylinder will now be derived because of their intrinsic interest and also to substantiate the thin-wall treatment and to find its limitations.

2. Thick-Wall Case

In order to determine the electric field within a thick-wall cylinder, equations (10) to (12) are again employed. The cylindrical harmonic may be written as (ref. 6)

$$\Phi(r,\theta,z) = \sum_m \sum_n (A_{mn} \sinh k_{mn}z + B_{mn} \cosh k_{mn}z)(C_{mn} \sin n\theta + D_{mn}\cos n\theta)$$
$$Z_n(k_{mn}r) + \sum_n (A_n \sin n\theta + B_n \cos n\theta)(C_n z + D_n)(E_n r^n + F_n r^{-n})$$
$$+ C_o \log_e r \qquad (22)$$

where

$$Z_n(k_{mn}r) = E_{mn}J_n(k_{mn}r) + F_{mn}Y_n(k_{mn}r) \tag{23}$$

and $J_n(\ )$ and $Y_n(\ )$ are Bessel functions of order n of the first and second kinds, respectively. For simplicity, λ will be taken to be $\pi/2$. From physical considerations it is apparent that only the component of the magnetic field normal to the spin axis is effective in generating a current; therefore, this restriction on λ will be inconsequential. By using equations (10) and (22), the components of the electric field vector within the conductor can be written as

$$E_r = \frac{\partial \phi}{\partial r}$$

$$= \sum_m \sum_n (A_{mn} \sinh k_{mn}z + B_{mn} \cosh k_{mn}z)(C_{mn} \sin n\theta + D_{mn} \cos n\theta)Z_n'(k_{mn}r)$$

$$+ \sum_n (A_{mn} \sin n\theta + B_n \cos n\theta)(C_n z + D_n)(E_n r^{n-1} - F_n r^{-n-1})n + \frac{C_0}{r} \tag{24}$$

$$E_\theta = \frac{\partial \phi}{r\partial \theta}$$

$$= \frac{1}{r}\sum_m \sum_n (A_{mn} \sinh k_{mn}z + B_{mn} \cosh k_{mn}z)(C_{mn} \cos n\theta - D_{mn} \sin n\theta)nZ_n(k_{mn}r)$$

$$+ \frac{1}{r}\sum_n (A_n \cos n\theta - B_n \sin n\theta)(C_n z + D_n)(E_n r^n + Fr^{-n})n \tag{25}$$

$$E_z = \frac{\partial \Phi}{\partial z} = c^{-1} h^{\omega} r \cos \theta$$

$$= \sum_m \sum_n k_{mn}(A_{mn} \cosh k_{mn} z + B_{mn} \sinh k_{mn} z)(C_{mn} \sin n\theta + D_{mn} \cos n\theta)$$

$$Z_n(k_{mn} r) + \sum_n C_n(A_n \sin n\theta + B_n \cos n\theta)(E_n r^n + F_n r^{-n}) = c^{-1} h^{\omega} r \cos \theta \tag{26}$$

The boundary conditions are now applied to the problem. First the requirement of equation (11) that the longitudinal component of the electric field vanish at the ends is applied to equation (26). By symmetry $B_{mn} = 0$. Also, only the cos θ terms can have nontrivial coefficients, that is, $D_{mn} = B_n = 0$ $(n \neq 1)$ and $C_{mn} = A_n = 0$. Next, the requirement of equation (12) that the radial component of the electric field vanish at the inside and outside surfaces is applied to equation (24). This condition gives $C_o = 0$, $C_n = F_n = 0$, and

$$Z_n'(k_{mn} r_o) = Z_n'(k_{mn} r_i) = 0 \tag{27}$$

Equations (27) yield the characteristic equation which determines the eigenvalues k_{mn} and also $\frac{F_{mn}}{B_{mn}}$. The method of evaluating them will be discussed presently. By letting $D_{m1} = 1$ and dropping the n subscript, equations (22), (24), (25), and (26) are reduced to

$$\Phi(r,\theta,z) = \sum_{m=1} A_m \sinh k_m z \cos \theta \, Z_1(k_m r) \tag{28}$$

$$E_r = \sum_{m=1} A_m \sinh k_m z \cos \theta \, Z_1'(k_m r) \tag{29}$$

$$E_\theta = -\sum_{m=1}^{\infty} A_m \sinh k_m z \sin\theta \, Z_1(k_m r) \tag{30}$$

$$E_z = \sum_{m=1}^{\infty} A_m k_m \cosh k_m z \cos\theta \, Z_1(k_m r) - c^{-1} h v_0 r \cos\theta \tag{31}$$

In order to evaluate k_m and $\frac{F_{mn}}{E_{mn}}$, equation (27) is expanded by means of equation (23) and then $Z_1'(k_m r)$ is replaced by $k_m Z_0(k_m r) - \frac{1}{r} Z_1(k_m r)$. The following two equations are thus obtained:

$$E_m\left[k_m J_0(k_m r_i) - \frac{1}{r_i} J_1(k_m r_i)\right] + F_m\left[k_m Y_0(k_m r_i) - \frac{1}{r_i} Y_1(k_m r_i)\right] = 0 \tag{32}$$

$$E_m\left[k_m J_0(k_m r_o) - \frac{1}{r_o} J_1(k_m r_o)\right] + F_m\left[k_m Y_0(k_m r_o) - \frac{1}{r_o} Y_1(k_m r_o)\right] = 0 \tag{33}$$

Eliminating $\frac{F_m}{E_m}$ between equations (32) and (33) gives the characteristic equation for the k_m values

$$\frac{k_m J_0(k_m r_o) - \frac{1}{r_o} J_1(k_m r_o)}{k_m Y_0(k_m r_o) - \frac{1}{r_o} Y_1(k_m r_o)} = \frac{k_m J_0(k_m r_i) - \frac{1}{r_i} J_1(k_m r_i)}{k_m Y_0(k_m r_i) - \frac{1}{r_i} Y_1(k_m r_i)} \tag{34}$$

One method of solving equation (34) is to rewrite it as

$$\frac{k_m r_o J_0(k_m r_o) - J_1(k_m r_o)}{k_m r_o Y_0(k_m r_o) - Y_1(k_m r_o)} = \frac{k_m r_i J_0(k_m r_i) - J_1(k_m r_i)}{k_m r_i Y_0(k_m r_i) - Y_1(k_m r_i)} \tag{35}$$

Now define $P(x)$ by

$$P(x) = \frac{x J_0(x) - J_1(x)}{x Y_0(x) - Y_1(x)}$$

Thus, the characteristic equation may be written as

$$P(k_m r_i) = P(k_m r_o) \tag{37}$$

A plot of the variation of $P(x)$ with x which is applicable for all cases can be made. To determine the eigenvalues for a cylinder with a given r_i/r_o, $P\left(\frac{r_i}{r_o} x\right)$ is plotted as a function of x. The intersections of $P\left(\frac{r_i}{r_o} x\right)$ with $P(x)$ satisfy equation (37) and, therefore, give the desired eigenvalues $k_m = \frac{\lambda_m}{r_o}$. Such a plot is shown in figure 5. The solid line is for $P(x)$ and the dashed line is for $P(0.5x)$ or $\frac{r_i}{r_o} = 0.5$. In this example, the first three eigenvalues given by the intersections are seen to be $k_m = 1.42$, 6.53, and 12.65, where r_o is assumed to be unity. The variations of the first few eigenvalues with r_i/r_o are shown in figure 6.

After the eigenvalues have been determined, F_m/E_m is given immediately by

$$\frac{F_m}{E_m} = - P(k_m r_o) \tag{38}$$

The variation of the first few values of F_m/E_m with r_i/r_o is shown in figure 7. The singular points occur where E_m becomes zero while F_m remains finite.

The A_m values are determined by again applying equation (11) to equation (31) and using the orthogonality properties of Bessel functions:

$$A_m = \frac{c^{-1} h \omega r_o a_m}{k_m \cosh \frac{k_m l}{2}} \tag{39}$$

where, by reference 7,

$$a_m = \frac{\int_{r_i}^{r_o} r\, Z_1(k_m r)\,dr}{r_o \int_{r_i}^{r_o} r\left[Z_1(k_m r)\right]^2 dr}$$

$$= \frac{\left.\frac{r^2}{k_m} Z_2(k_m r)\right|_{r_i}^{r_o}}{\left.r_o \frac{r^2}{2}\left\{\left[Z_1(k_m r)\right]^2 - Z_o(k_m r) Z_2(k_m r)\right\}\right|_{r_i}^{r_o}} \tag{40}$$

The a_m values are thus nondimensional and are functions only of r_i/r_o for a given m. It is noted that E_m and F_m need not be separately determined; only their ratio F_m/E_m need be found. Substituting equation (39) into equations (28) to (31) gives

$$\phi(r,\theta,z) = c^{-1} h \omega r_o \cos\theta \sum_{m=1}^{\infty} \frac{a_m}{k_m} \frac{\sinh k_m z}{\cosh \frac{k_m \ell}{2}} Z_1(k_m r) \tag{41}$$

$$E_r = c^{-1} h \omega r_o \cos\theta \sum_{m=1}^{\infty} \frac{a_m}{k_m} \frac{\sinh k_m z}{\cosh \frac{k_m \ell}{2}} Z_1'(k_m r) \tag{42}$$

$$E_\theta = -c^{-1} h \omega \frac{r_o}{r} \sin\theta \sum_{m=1}^{\infty} \frac{a_m}{k_m} \frac{\sinh k_m z}{\cosh \frac{k_m \ell}{2}} Z_1(k_m r) \tag{43}$$

$$E_z = -c^{-1} h \omega r_o \cos\theta \left[\frac{r}{r_o} - \sum_{m=1}^{\infty} a_m \frac{\cosh k_m z}{\cosh \frac{k_m \ell}{2}} Z_1(k_m r)\right] \tag{44}$$

The electric field is, therefore, determined within the cylinder. The convergence of these summations is generally good.

The procedure for determining the torque is essentially the same as outlined before for the thin-wall cylindrical shell. The result is

$$\bar{L} = \pi\sigma c^{-2}h^2 \sin\lambda\, \omega l r_o^4 \left\{ \frac{1}{4}\left[1 - \left(\frac{r_i}{r_o}\right)^4\right] - \sum_{m=1}^{\infty} \frac{\beta_m}{k_m' \frac{l}{2r_o}} \tanh\left(k_m' \frac{l}{2r_o}\right) \right\} (\bar{i}\cos\lambda - \bar{k}\sin\lambda) \qquad (45)$$

where $l/2r_o$ is the fineness ratio, k_m' is the eigenvalue nondimensionalized with respect to r_o, that is, $k_m' = r_o k_m$, and β_m is defined by

$$\beta_m = \frac{a_m}{r_o^3}\int_{r_i}^{r_o} r^2 Z_1(k_m r)\,dr = \frac{a_m}{r_o^3}\left[\frac{r^2}{k_m} Z_2(k_m r)\right]\Bigg|_{r_i}^{r_o} \qquad (46)$$

Note that again, for large values of the fineness ratio $l/2r_o$, the torque per unit length is independent of the fineness ratio.

The torque per unit length per unit thickness as a function of r_i/r_o is shown in figure 8 for various fineness ratios. (The product $\sigma c^{-2}h^2\omega r_o^4$ is taken to be unity.) Figure 9 is a cross plot showing the torque per unit length per unit thickness as a function of fineness ratio for various r_i/r_o values. The $\frac{r_i}{r_o} = 1.0$ curve is identical to that for the thin-wall solution shown in figure 2.

C. THIN-WALL TUMBLING CYLINDER

The coordinate systems used in the analysis of the tumbling cylinder are shown in figure 10. The ξ, η, ζ coordinate system, with the unit vectors $\bar{e}_1$, $\bar{e}_2$, and $\bar{e}_3$, is space fixed at the center of the rotating cylinder, with the ξ-axis parallel to the spin axis and the ζ-axis oriented so that the magnetic field vector lies in the ξ, ζ plane. The

X, Y, Z system with unit vectors $\bar{I}$, $\bar{J}$, and $\bar{K}$ is fixed in the cylinder with the origin at the center of the cylinder, the X-axis being alined with the ξ-axis, and is rotated from the space-fixed system by the angle μ. In addition, a polar coordinate system r, θ, z with unit vectors $\bar{u}_r$, $\bar{u}_\theta$, and $\bar{u}_z$ is fixed in the cylinder, θ being measured from the X-axis, as in figure 1.

Now, because only the normal component of $\nabla \times \bar{J}$ is effective in a thin-wall conductor and radial currents are negligible, equations (1) and (4) give for this case

$$(\nabla \times \bar{J})_r = \frac{\partial J_z}{r\partial\theta} - \frac{\partial J_\theta}{\partial z} = -\sigma c^{-1} h\omega \sin\lambda \cos\mu \sin\theta \tag{47}$$

The continuity requirement (eq. (2)) reduces to

$$\nabla \cdot \bar{J} = \frac{\partial J_\theta}{r\partial\theta} + \frac{\partial J_z}{\partial z} = 0 \tag{48}$$

Radial current having been neglected, the boundary condition is simply

$$J_z = 0 \qquad \left(z = \pm \frac{l}{2}\right) \tag{49}$$

This problem could be solved by a scalar potential as before. However, to demonstrate an alternate approach, the solution will be by means of a stream function. With a stream function ψ defined as before (see eq. (20)),

$$\nabla^2\psi = -(\nabla \times \bar{J})_r \tag{50}$$

so that, by equation (47)

$$\nabla^2\psi = \frac{\partial^2\psi}{r^2\partial\theta^2} + \frac{\partial^2\psi}{\partial z^2} = \sigma c^{-1} h\omega \sin\lambda \cos\mu \sin\theta \tag{51}$$

Solving equation (51) yields

$$\psi = \sigma c^{-1} h \omega r^3 \sin\lambda \cos\mu \sin\theta + \sum_{n=0}^{\infty} (A_n \sin n\theta + B \cos n\theta)\left(C_n \sinh\frac{nz}{r} + D_n \cosh\frac{nz}{r}\right) \qquad (52)$$

Only the $\sin\theta$ component of the harmonic part of ψ will not vanish when the boundary condition is applied; therefore, $A_n = 0$ $(n > 1)$ and $B_n = 0$. By symmetry $C_n = 0$. The current density is then calculated by equations (50) and (52), under the condition that the longitudinal component vanish at the ends (eq. (49)), and $A_1 D_1$ is thereby determined. Thus the stream function and current components are shown to be

$$\psi(\theta,z) = \sigma c^{-1} h \omega r^3 \sin\lambda \cos\mu \left(1 - \frac{\cosh\frac{z}{r}}{\cosh\frac{l}{2r}}\right)\sin\theta \qquad (53)$$

$$J_\theta = \sigma c^{-1} h \omega r^2 \sin\lambda \cos\mu \frac{\sinh\frac{z}{r}}{\cosh\frac{l}{2r}} \sin\theta \qquad (54)$$

$$J_z = \sigma c^{-1} h \omega r^2 \sin\lambda \cos\mu \left(1 - \frac{\cosh\frac{z}{r}}{\cosh\frac{l}{2r}}\right)\cos\theta \qquad (55)$$

The torque resulting from this current is

$$\bar{L} = \pi\sigma c^{-2} h^2 \omega \sin\lambda\, r^3 l r \left(1 - \frac{2r}{l}\tanh\frac{l}{2r}\right)\cos\mu\,(-\bar{i}\sin\lambda\cos\mu + \bar{k}\cos\lambda) \qquad (56)$$

Expressed in space-fixed axes,

$$\bar{L} = \pi\sigma c^{-2}h^2\omega \sin\lambda\, r^3 l\tau\left(1 - \frac{2r}{l}\tanh\frac{l}{2r}\right)\left(-\bar{e}_1 \sin\lambda\cos^2\mu - \bar{e}_2 \cos\lambda \sin\mu\cos\mu + \bar{e}_3 \cos\lambda\cos^2\mu\right) \quad (57)$$

Averaging this torque around one revolution gives simply

$$\bar{L}_{av} = \frac{\pi}{2}\sigma c^{-2}h^2\omega \sin\lambda\, r^3 l\tau\left(1 - \frac{2r}{l}\tanh\frac{l}{2r}\right)\left(-\bar{e}_1 \sin\lambda + \bar{e}_3 \cos\lambda\right) \quad (58)$$

Comparison of equation (58) for a tumbling cylinder with equation (19) for a symmetrically spinning cylinder shows the two expressions to be identical except for a factor of 1/2 in the case of the tumbling cylinder because of the sinusoidal variation of the current. Also, it is seen from equations (21) and (5) that the streamlines are identical.

D. THIN-WALLED CONES AND CONIC FRUSTUMS

In studying the magnetic torques on thin-walled symmetrically spinning cones and cone frustums, coordinate systems are set up as shown in figure 11. Cartesian and polar coordinates are oriented as before, the Z-axis being parallel to $\bar{\omega}$, the X, Z plane containing $\bar{H}$, θ being measured in the X, Y plane from the X-axis, and r being measured normal to the Z-axis. The origin is placed at the vertex of the cone. The cone half-angle is ϕ. In addition, ρ is defined as the distance from the vertex to a point on the cone, and unit vectors $\bar{u}_\phi$ and $\bar{u}_\rho$ are defined normal to ρ and $\bar{u}_\theta$ and parallel to ρ, respectively.

As before, only the component of $\nabla \times \bar{J}$ normal to the surface is considered. Equation (1) gives

$$(\nabla \times \vec{J})_{\phi} = -\sigma c^{-1} h\omega \sin \lambda \cos \phi \sin \theta \qquad (59)$$

which is the governing equation for a conical surface.

As with the cylinder, the cone or cone frustum is a developable surface and can be rolled out on a plane; therefore, the problem becomes a boundary-value problem in a sector of an annulus or of a circle in a plane. The polar coordinates in the plane are the radial distance ρ and the central angle ν, which is related to the angle θ by the equation

$$\nu = \theta \sin \phi \qquad (60)$$

(This equation is readily verified by noting that a circumferential distance $(\rho \sin \phi)\theta$ on the cone becomes $\rho\nu$ in the plane.)

In polar coordinates, the Laplacian of the stream function is given by

$$\nabla^2 \psi = \frac{\partial^2 \psi}{\partial \rho^2} + \frac{\partial \psi}{\rho \, \partial \rho} + \frac{\partial^2 \psi}{\rho^2 \partial \nu^2}$$

so that equation (59) now becomes, with the aid of equation (60),

$$\frac{\partial^2 \psi}{\partial \rho^2} + \frac{\partial \psi}{\rho \, \partial \rho} + \frac{1}{\rho^2 \sin^2 \phi} \frac{\partial^2 \psi}{\partial \theta^2} = \sigma c^{-1} h\omega \sin \lambda \cos \phi \sin \theta \qquad (61)$$

As in the case of symmetrically spinning cylinders, only the $\sin \theta$ term of ψ remains after the boundary conditions have been applied.

Accordingly, the solution of equation (61) is assumed to be of the form

$$\psi(\rho, \theta) = \sin \theta \, f(\rho) \qquad (62)$$

Substituting this expression into equation (61) and rewriting gives

$$\rho^2 \frac{d^2 f}{d\rho^2} + \rho \frac{df}{d\rho} - \csc^2\phi \, f = \sigma c^{-1} h\omega \sin\lambda \cos\phi \, \rho^2 \qquad (63)$$

The result is seen to be an equidimensional equation. Substituting the solution for $f(\rho)$ into equation (62) gives

$$\psi(\rho, \theta) = \frac{\sigma c^{-1} h\omega \sin\lambda \cos\phi \sin\theta}{4 - \csc^2\phi} \left(\rho^2 + A\rho^{\csc\phi} + B\rho^{-\csc\phi} \right) \qquad (64)$$

where A and B are to be determined.

The two components of current density are

$$\frac{\partial \psi}{\partial \rho} = J_\theta(\rho, \theta)$$

$$= \frac{\sigma c^{-1} h\omega \sin\lambda \cos\phi \sin\theta}{4 - \csc^2\phi} \left(2\rho + A \csc\phi \, \rho^{\csc\phi - 1} - B \csc\phi \, \rho^{-\csc\phi - 1} \right)$$

(65)

$$-\frac{1}{\rho \sin\phi} \frac{\partial \psi}{\partial \theta} = J_\rho(\rho, \theta)$$

$$= -\frac{\sigma c^{-1} h\omega \sin\lambda \cot\phi \cos\phi}{4 - \csc^2\phi} \left(\rho + A\rho^{\csc\phi - 1} + B\rho^{-\csc\phi - 1} \right)$$

(66)

In applying these equations to a cone, the boundary conditions are that $\overline{J}\rho = 0$ at the end $\rho = \rho_a$ and that the current density remains finite throughout the cone. By the latter condition $B = 0$, and the former gives

$$\rho_a + A\rho_a^{\csc\phi - 1} = 0$$

or

$$A = -\rho_a^{2-\csc\phi} \tag{67}$$

For a cone frustum, it is required that $J_\rho = 0$ at both ends, $\rho = \rho_a$ and $\rho = \rho_b$. Thus

$$\rho_a + A\rho_a^{\csc\phi - 1} + B\rho_a^{-\csc\phi - 1} = 0 \tag{68a}$$

$$\rho_b + A\rho_b^{\csc\phi - 1} + B\rho_b^{-\csc\phi - 1} = 0 \tag{68b}$$

Simultaneous solution of these two equations gives

$$A = \frac{\rho_a^{-\csc\phi - 1}\rho_b - \rho_a\rho_b^{-\csc\phi - 1}}{\rho_a^{\csc\phi - 1}\rho_b^{-\csc\phi - 1} - \rho_a^{-\csc\phi - 1}\rho_b^{\csc\phi - 1}} \tag{69a}$$

$$B = \frac{\rho_a\rho_b^{\csc\phi - 1} - \rho_a^{\csc\phi - 1}\rho_b}{\rho_a^{\csc\phi - 1}\rho_b^{-\csc\phi - 1} - \rho_a^{-\csc\phi - 1}\rho_b^{\csc\phi - 1}} \tag{69b}$$

Substitution of the current expressions (eqs. (65) and (66)) into equation (18) gives the torque

$$\bar{L} = \frac{\pi\sigma c^{-2}h^2\omega \sin\lambda \cos^2\phi \sin\phi \tau}{4 - \csc^2\phi}\left(\frac{\rho^4}{4} + \frac{A\rho^{\csc\phi + 2}}{\csc\phi + 2} + \frac{B\rho^{-\csc\phi + 2}}{-\csc\phi + 2}\right)\Bigg|_{\rho_a}^{\rho_b}(-\bar{I}\cos\lambda + \bar{k}\sin\lambda) \tag{70}$$

It is seen that the solution in the form given here contains a singularity for $\csc\phi = \pm 2$ or $\phi = \pm 30^\circ$. This is due to the homogeneous part of the solution becoming identical with the inhomogeneous part. The solution for this case may be obtained by introducing a transformation variable w defined by

$$\left.\begin{aligned} \rho &= e^{w} \\ w &= \log_e \rho \end{aligned}\right\} \qquad (71)$$

whence

$$\rho \frac{df}{d\rho} = \frac{df}{dw}$$

$$\rho^2 \frac{d^2f}{d\rho^2} = \frac{d^2f}{dw^2} - \frac{df}{dw}$$

With these expressions, equation (63) gives, for $\phi = \pm 30^\circ$,

$$\frac{d^2f}{dw^2} - 4f = \sigma c^{-1} h^{w} \sin \lambda \frac{\sqrt{3}}{2} e^{2w}$$

The solution of this equation is

$$f = \frac{\sqrt{3}}{8} \sigma c^{-1} h^{w} \sin \lambda \left(we^{2w} + Ae^{2w} + Be^{-2w} \right)$$

$$= \frac{\sqrt{3}}{8} \sigma c^{-1} h^{w} \sin \lambda \left(\rho^2 \log_e \rho + A\rho^2 + B\rho^{-2} \right) \qquad (72)$$

The stream function is thus given by

$$\psi(\rho, \theta) = \frac{\sqrt{3}}{8} \sigma c^{-1} h^{w} \sin \lambda \sin \theta \left(\rho^2 \log_e \rho + A\rho^2 + B\rho^{-2} \right) \qquad (73)$$

and the current density components are

$$J_\theta(\rho, \theta) = \frac{\sqrt{3}}{8} \sigma c^{-1} h^{w} \sin \lambda \sin \theta \left[\rho(1 + \log_e \rho) + 2A\rho - 2B\rho^{-3} \right] \qquad (74)$$

$$J\rho(\rho, \theta) = -\frac{\sqrt{3}}{4} \sigma c^{-1} h^{w} \sin \lambda \cos \theta \left(\rho \log_e \rho + A\rho + B\rho^{-3} \right) \qquad (75)$$

As before, these equations are applied to a cone, and the constants are found to be

$$A = - \log_e \rho_a$$

$$B = 0$$

Likewise, for a frustum, the constants are

$$A = \frac{\rho_b^4 \log_e \rho_b - \rho_a^4 \log_e \rho_a}{\rho_a^4 - \rho_b^4}$$

$$B = \frac{\rho_a^4 \rho_b^4 (\log_e \rho_a - \log_e \rho_b)}{\rho_a^4 - \rho_b^4}$$

The resultant torque is then

$$\bar{L} = \frac{3}{16} \pi \sigma c^{-2} h^2 \omega \sin \lambda \, \tau \left[\frac{1}{3} \rho^3 \left(\log_e \rho - \frac{1}{3} \right) + \frac{1}{2} A \rho^2 - \frac{1}{2} B \rho^{-2} \right] (\bar{i} \cos \lambda - \bar{k} \sin \lambda) \qquad (76)$$

E. SERIES OF CONE FRUSTUMS

If a series of m conic frustums are joined end to end, as in figure 12, equations (64), (65), and (66) apply in each section, and it remains only to determine the A and B for each section in order to define fully the current and hence the torque. At the joint, the radial component of current must be continuous, and the circumferential component must also be continuous as otherwise a vortex line would be formed, with resulting infinite curl of current along the joint. Therefore, the conditions for determining the constants are that the respective components of current are continuous at the joints, and that at an open end the radial component vanishes, or that, if the end is closed by a cone, the current remains finite. With the notation for the ends of each

section as shown in figure 12, these conditions can be written for the junctions as

$$J_\rho(\rho_{nb}, \theta) = J_\rho(\rho_{n+1,a}, \theta) \tag{77a}$$

$$J_\theta(\rho_{nb}, \theta) = J_\theta(\rho_{n+1,a}, \theta) \tag{77b}$$

By using equations (65) and (66), equations (77) become

$$A_n a_{nb} + B_n b_{nb} + c_{nb} = A_{n+1} a_{n+1,a} + B_{n+1} b_{n+1,a} + c_{n+1,a} \tag{78a}$$

$$A_n a_{nb} - B_n b_{nb} + f_{nb} = A_{n+1} a_{n+1,a} - B_{n+1} b_{n+1,a} + f_{n+1,a} \tag{78b}$$

where

$$a_{na} = \frac{\rho_{na}^{\csc \phi_n - 1} \cot \phi_n}{4 - \csc^2 \phi_n} \tag{79a}$$

$$b_{na} = \frac{\rho_{na}^{-\csc \phi_n - 1} \cot \phi_n}{4 - \csc^2 \phi_n} \tag{79b}$$

$$c_{na} = \frac{\rho_{na} \cot \phi_n}{4 - \csc^2 \phi_n} \tag{79c}$$

$$f_{na} = \frac{2\rho_{na} \cos \phi_n}{4 - \csc^2 \phi_n} \tag{79d}$$

and a_{nb}, b_{nb}, c_{nb}, and f_{nb} are similarly defined. The two parts of equation (78) give, by addition and subtraction

$$A_n a_{nb} + \frac{c_{nb} + f_{nb}}{2} = A_{n+1} a_{n+1,a} + \frac{c_{n+1,a} + f_{n+1,a}}{2} \qquad (80a)$$

$$B_n b_{nb} + \frac{c_{nb} - f_{nb}}{2} = B_{n+1} b_{n+1,a} + \frac{c_{n+1,a} - f_{n+1,a}}{2} \qquad (80b)$$

In the application of these equations, it is important to note that, in proceeding from one end of the frustum series to the other, if the opening angle of a cone with radius increasing with the distance along the body is considered positive, the opening angle of a cone with radius decreasing as z increases must be negative, and vice versa. This sign convention is intrinsically assumed by the equations.

Equations (80) furnish $2m - 2$ of the equations necessary for the determination of the $2m$ constants. In order to set up the remaining two equations, it is necessary to consider the following three cases, each of which must be treated separately:

1. Both ends closed: in this case, finiteness requires that

$$B_1 = 0 \qquad (81a)$$

$$A_m = 0 \qquad (81b)$$

Equation (81a) provides an initial vlaue from which successive B_n values can be calculated by the recurrence equation (80b). Likewise the A_n values can be determined by equations (80a) and (81b).

2. One end open and one end closed: at the closed end, finiteness requires that

$$B_1 = 0$$

and, at the open end, the requirement that the longitudinal current vanish gives equation (68b) applied to the mth segment. Thus, the B_n values can again be calculated by recurrence, after which equation (68b) gives A_m, and the A_n values can then be determined similarly.

3. Both ends open: the boundary conditions for this case are that the radial component of the current vanish at each end, so that equations (68a) and (68b) are applied to the first and last segments, respectively. Next A_m and B_m are expressed by linear relations in A_1 and B_1, respectively, obtained by successive use of equations (80a) and (80b). Equations (68a) and (68b) now become a pair of simultaneous equations in A_1 and B_1, so that these two can be found. The others then follow.

The constants in the current equations having been determined, the flow is completely defined and the torque follows by summing the contributions of all the sections, each being determined by equation (70).

F. GENERAL THIN-WALL BODY OF REVOLUTION

The next step is to apply the theory developed for series of frustums to the case of a continuous body of revolution (fig. 13) having as generatrix an arbitrary curve, say $r = r(z)$, which has a piecewise continuous first derivative dr/dz. Initially, however, it will be assumed that dr/dz is continuous throughout the length of the body.

The body is considered as made up of a large number of frustums joined; therefore, equations (80) apply. Equation (80a) is now

rewritten in the following form (for a reason that will be immediately apparent)

$$A_{n+1}a_{n+1,a} - A_n a_{nb} = \frac{1}{2}\left[(c_{nb} - c_{n+1,a}) + (f_{nb} - f_{n+1,a})\right] \qquad (82)$$

If the body is considered to be continuously curved,

$$A_{n+1} = A_n + \frac{dA_n}{dz}\Delta z_n$$

$$a_{n+1,a} = a_{nb} + \frac{da_n}{dz}\Delta z_n$$

With these expressions, equation (82) becomes, in the limit

$$d\left[a(z)A(z)\right] = -\frac{1}{2}\left[dc(z) + df(z)\right] \qquad (83)$$

The subscripts are no longer needed, as A, a, c, and f are continuous functions of z. Equation (83) may be integrated directly to give

$$a(z)A(z) = -\frac{c(z) + f(z)}{2} + a(0)A(0) + \frac{c(0) + f(0)}{2} \qquad (84)$$

or

$$A(z) = a^{-1}(z)\left[a(0)A(0) + \frac{c(0) + f(0)}{2} - \frac{c(z) + f(z)}{2}\right] \qquad (85)$$

Similarly

$$B(z) = b^{-1}(z)\left[b(0)B(0) + \frac{c(0) - f(0)}{2} - \frac{c(z) - f(z)}{2}\right] \qquad (86)$$

The quantities a, b, c, and f are defined by equations (79) as functions of ρ and ϕ. These are defined in terms of r(z) by the geometry of the problem, as shown in figure 13, as

$$\rho = r\sqrt{1 + \left(\frac{dr}{dz}\right)^{-2}} \tag{87}$$

$$\phi = \tan^{-1}\left(\frac{dr}{dz}\right) \tag{88}$$

Other needed relations that follow from figure 13 are

$$\csc^2\phi = 1 + \left(\frac{dr}{dz}\right)^{-2}$$

$$\cot\phi = \left(\frac{dr}{dz}\right)^{-1}$$

The constants A(0) and B(0) are determined in the same manner as that outlined for the joined frustums, in order to satisfy the condition that no current flows out the ends. The functions A(z) and B(z) thus evaluated are substituted into equations (64), (65), and (66) to obtain the stream function and current components. The torque then follows as

$$\bar{L} = \pi\sigma c^{-2}h^2\omega_k \int_{\rho_a}^{\rho_b} \frac{\cos^2\phi \sin\phi}{4 - \csc^2\phi}\left[\rho^3 + A(z)\rho^{\csc\phi+1} + B(z)\rho^{-\csc\phi+1}\right]d\rho \tag{89}$$

In general, this integral would have to be evaluated numerically. Any discontinuities in the slope are accounted for merely by treating the discontinuity as a juncture in a series of frustums.

VII. ANALYSIS, PART II

A. SPACE FIXED DIPOLE FIELD

The torque due to eddy currents acting on a satellite is shown by Vinti, reference 5, to be

$$\overline{M} = K(\overline{\omega} \times \overline{H}) \times \overline{H} \tag{1}$$

where K is a constant for the satellite spinning about a given body axis. (Small variations of K due to effects such as change of conductivity with satellite temperature are neglected in this thesis.) Equation (1) can be rewritten as

$$\overline{M} = K\left[\overline{HH} - H^2\,\overline{\overline{I}}\right] \cdot \overline{\omega} \tag{2}$$

or in matrix notation, is expressed by

$$\begin{Bmatrix} M_x \\ M_y \\ M_z \end{Bmatrix} = K \begin{bmatrix} -(H_y^2 + H_z^2) & H_xH_y & H_xH_z \\ H_yH_x & -(H_z^2 + H_x^2) & H_yH_z \\ H_zH_x & H_zH_y & -(H_x^2 + H_y^2) \end{bmatrix} \begin{Bmatrix} \omega_x \\ \omega_y \\ \omega_z \end{Bmatrix} \tag{3}$$

For reasonable configurations, the time required for the spin to decrease to one-half its original value due to eddy current torques is on the order of one hundred days (refs. 1 through 5). Hence, during a day, the change in spin rate is on the order of one percent, and during a single orbit, roughly two hours, the spin vector is very nearly constant. Thus, integrating the torque with respect to time over one orbit and dividing by the period gives the average torque acting on the satellite as

$$\overline{M}_{av} = \frac{1}{P}\int_0^P \overline{T}\, dt = \frac{K}{P}\int_0^P \left[\overline{HH} - H\,\overline{\overline{I}}\right] \cdot \overline{\omega}\, dt = \frac{K}{P}\overline{\overline{A}}' \cdot \overline{\omega} \qquad (4)$$

where the dyad $\overline{\overline{A}}'$ may be expressed by a matrix, A', as

$$A' = \int_0^P \begin{bmatrix} -(H_y^2 + H_z^2) & H_xH_y & H_xH_z \\ H_yH_x & -(H_z^2 + H_x^2) & H_yH_z \\ H_zH_x & H_zH_y & -(H_x^2 + H_y^2) \end{bmatrix} dt$$

It is next necessary to evaluate the elements of A'.

The geomagnetic field is assumed to be a dipole field and the tilt of the axis of the dipole with respect to the spin axis of the earth is neglected, so that the field is not a function of longitude and time. The magnetic field is thereby a function of position of the satellite, which is given by the classical orbit relations.

A Cartesian coordinate system is defined, with the z-axis along the dipole axis and the x-axis passing through the ascending node of the intersection of the orbit plane with the geomagnetic equatorial plane. The y-axis then completes the orthogonal coordinate system, as shown in figure 14. The orbit plane is described with respect to this system by the angle of inclination to the geomagnetic equator, i, and the argument of the perigee, η. The position of the satellite in its orbit is given by the orbit angle θ, or by the longitude ϕ and colatitude ψ within the coordinate system chosen.

The spherical components of a dipole field of strength ρ are

$$H_r = \frac{2\,s\cos\psi}{r^3} \qquad (5a)$$

$$H_\psi = \frac{s\sin\psi}{r^3} \qquad (5b)$$

or, in Cartesian coordinates

$$\begin{Bmatrix} H_x \\ H_y \\ H_z \end{Bmatrix} = \frac{s}{r^3} \begin{Bmatrix} 3 \sin \psi \cos \psi \cos \phi \\ 3 \sin \psi \cos \psi \sin \phi \\ 3 \cos^2 \psi - 1 \end{Bmatrix} \tag{6}$$

Orbit mechanics give the equations

$$\dot{\theta} = \frac{\sqrt{mp}}{r^2} \tag{7}$$

and

$$r = \frac{p}{1 + \epsilon \cos \theta} \tag{8}$$

The angles ψ and ϕ are given by

$$\cos \psi = \sin i \sin (\theta + \eta) \tag{9}$$

and

$$\tan \phi = \cos i \tan (\theta + \eta) \tag{10}$$

The variable of integration in equation (4) is changed to θ, thus

$$\overline{M} = \frac{1}{P}\int_0^P \overline{M}\, dt = \frac{1}{P}\oint \frac{\overline{M}}{\dot{\theta}}\, d\theta = \frac{1}{P\sqrt{mp}} \oint \overline{M}\, r^2\, d\theta \tag{11}$$

and

$$A' = \frac{1}{\sqrt{mp}} \oint \begin{bmatrix} -(H_y^2 + H_z^2) & H_xH_y & H_xH_z \\ H_yH_x & -(H_z^2 + H_x^2) & H_yH_z \\ H_zH_x & H_zH_y & -(H_x^2 + H_y^2) \end{bmatrix} r^2\, d\theta$$

Equations (8), (9), and (10) are used, after extensive manipulation, in equation (6) to express the components of $\overline{\overline{H}}$ as functions of θ and the orbit parameters p, ϵ, i, and η. These expressions are substituted into equation (12) and the integration performed. It is found that the first and third order eccentricity terms vanish; the second and fourth order terms, in part, contain the factors $\cos 2\eta$ and 4η, respectively. When terms only of zero order in eccentricity are retained, the A' matrix is found to reduce to

$$A' = -\frac{2\pi}{\sqrt{mp}}\frac{s^2}{p^4}A(i) \tag{13}$$

where

$$A(i) = \begin{bmatrix} \alpha(i) & 0 & 0 \\ 0 & \beta(i) & \delta(i) \\ 0 & \delta(i) & \gamma(i) \end{bmatrix}$$

$$= \begin{bmatrix} \left(1\frac{3}{8} - \frac{3}{8}\cos^2 i\right) & 0 & 0 \\ 0 & \left(2\frac{1}{2} - 4\frac{7}{8}\cos^2 i + 3\frac{3}{8}\cos^4 i\right) & \left(3\frac{3}{8}\sin^3 i\cos i\right) \\ 0 & \left(3\frac{3}{8}\sin^3 i\cos i\right) & \left(1\frac{1}{8} + 2\frac{1}{4}\cos^2 i - 3\frac{3}{8}\cos^4 i\right) \end{bmatrix} \tag{14}$$

Figure 15 shows the elements of $A(i)$ as a function if inclination, i.

The orbital period is replaced by $\dfrac{2\pi p^{3/2}}{m^{1/2}(1-\epsilon^2)^{3/2}}$, and the ϵ^2 term neglected, so that equation (4) for the average torque due to eddy currents becomes

$$\{M_{av}\} = -\frac{Ks^2}{p^6}A(i)\{\omega\} \tag{15}$$

This torque may be added to other torques, for example, due to gravitation gradients, in order to study the motion of a satellite. In the present thesis, however, the only external torque considered is that due to eddy currents.

It is well known that for spinning satellites, because of internal dissipation of kinetic energy of rotation, the only stable axis of rotation is the axis of maximum momentum (ref. 8). Hence, the angular momentum of the satellite is simply $I_{max} \{\omega\}$, and the equation of the spin motion of the satellite becomes

$$I_{max} \{\dot{\omega}\} = -\frac{Ks^2}{p^6} A(i) \{\omega\} \tag{16}$$

The solution form

$$\{\omega\} = \{\omega_0\} \exp\left(-\frac{K s^2}{I_{max} p^2}\right) \lambda t$$

is substituted into equation (16), whence

$$A(i) \{\omega\}_0 = \lambda \{\omega\}_0$$

or

$$(A_{(i)} - \lambda I) \{\omega\}_0 = 0 \tag{17}$$

which is simply a matrix eigenvalue problem. Equation (17) has non-trivial solutions only if

$$\det \left| (A_{(i)} - \lambda I \right| = \begin{vmatrix} \alpha - \lambda & 0 & 0 \\ 0 & \beta - \lambda & \delta \\ 0 & \delta & \gamma - \lambda \end{vmatrix} = 0 \tag{18}$$

It is noted that the x-component is uncoupled from the y- and z-components, that is, all terms in the first column and first row vanish, except $(\alpha - \lambda)$, which simplifies the problem considerably. The three solutions of equation (18) are

$$\left.\begin{aligned} \lambda_1 &= \alpha \\ \lambda_{2,3} &= \frac{\beta + \gamma}{2} \pm \sqrt{\frac{\beta + \gamma^2}{2} + (\delta^2 - \beta\gamma)} \\ &= \frac{\beta + \gamma}{2} \pm \sqrt{\frac{\beta - \gamma^2}{2} + \delta^2} \end{aligned}\right\} \qquad (19)$$

The eigenvalues are plotted in figure 16 as a function of orbital inclination.

The components of the corresponding unit eigenvectors are the minors of $\det \left| A(i) - \lambda I \right|$ obtained by moving across a row, and normalizing, and are

$$e_1 = \begin{Bmatrix} 1 \\ 0 \\ 0 \end{Bmatrix}$$

$$e_2 = \left[(\gamma - \lambda_2)^2 + \delta^2\right]^{-1/2} \begin{Bmatrix} 0 \\ \lambda_2 - \gamma \\ \delta \end{Bmatrix} \qquad (20)$$

$$e_3 = \left[(\beta - \lambda_3)^2 + \delta^2\right]^{-1/2} \begin{Bmatrix} 0 \\ -\delta \\ \beta - \lambda_3 \end{Bmatrix}$$

The matrix $(A_{(1)} - \lambda I)$ is seen to be symmetric, hence the eigenvectors are orthogonal. This affords a considerable simplification to the calculations. Since e_1 coincides with the x-axis, then e_2 and e_3 are obtained by rotating $\bar{j}$ and $\bar{k}$, respectively, through some angle, χ, as shown in figure 17. Hence

$$e_2 = \begin{Bmatrix} 0 \\ \cos\chi \\ +\sin\chi \end{Bmatrix} \text{ and } e_3 = \begin{Bmatrix} 0 \\ -\sin\chi \\ \cos\chi \end{Bmatrix} \tag{21}$$

A comparison of equations (20) and (21) shows that

$$\text{Tan}\,\chi = \frac{\delta}{\tau - \lambda_2} \tag{22}$$

and the angle of rotation, χ, is shown as a function of orbital inclination in figure 18. Finally, the spin vector may be written as a linear combination of the solutions to equation (16)

$$\bar{\omega} = a_1 e_1 e^{-\lambda_1 \tau} + a_2 e_2 e^{-\lambda_2 \tau} + a_3 e_3 e^{-\lambda_3 \tau} \tag{23}$$

where

$$\tau = \left(\frac{K}{I_{max}} \frac{s^2}{p^6}\right) t \tag{24}$$

The a_i's are the components of $\bar{\omega}_o$ expressed in the e_i system, and can be written as

$$\begin{Bmatrix} a_1 \\ a_2 \\ a_3 \end{Bmatrix} = \begin{bmatrix} 1 & 0 & 0 \\ 0 & \cos \chi & \sin \chi \\ 0 & -\sin \chi & \cos \chi \end{bmatrix} \begin{Bmatrix} \omega_{x_o} \\ \omega_{y_o} \\ \omega_{z_o} \end{Bmatrix} \qquad (25)$$

Thus far, it has been assumed, for simplicity, that the geomagnetic field is a dipole with the axis along the earth's spin axis. Consideration is now given to the effects produced by tilting the dipole axis with respect to the earth's spin axis.

B. ROTATING EARTH WITH TILTED DIPOLE FIELD

The geomagnetic field of the earth is approximated by a dipole field, with the dipole axis tilted 17°, with respect to the earth's spin axis.(ref. 7).

In order to include the effect of the tilt of the magnetic dipole field, with respect to the earth's spin axis, it is necessary to define three coordinate systems. The space fixed, or inertial system, $x_I\ y_I\ z_I$ is oriented with the z_I-axis along the earth's spin axis, and the x_I-axis along the intersection of the satellite orbit plane with the equator, thus the x_I-axis passes through the ascending node. The earth fixed axis system, $x_E\ y_E\ z_E$, is oriented so that the z_E-axis is along the earth's spin axis and the x_E-axis passes through the intersection of the equator with the geomagnetic equator. Finally, the geomagnetic axis system, $x_M\ y_M\ z_M$, is defined, with the z_M-axis along the axis of the geomagnetic dipole, and the x_M-axis passing through the ascending node of the orbit referenced to the geomagnetic

equator. Several angles are defined: i_I denotes the orbital inclination with respect to the earth's equator and i_M the orbital inclination with respect to the geomagnetic equator; μ is the angle between the x_I- and x_E-axes; ν is the angle between the x_M- and x_E-axes; and ζ is the tilt of the dipole field with respect to the earth's spin axis, that is, the angle between z_E and z_M. These are shown in figure 19. It is seen that these angles are all related, in the spherical triangle, ABC. The purpose of each coordinate system is as follows:

The inertial coordinate system provides the necessary fixed reference, as the other coordinate systems rotate with the earth. The analysis of the previous section was referenced to the geomagnetic coordinate system. The earth-fixed system serves as an intermediate coordinate system by which Euler angle rotations are made in transforming from the inertial to the geomagnetic coordinate system, and is further necessitated by the requirement that $\frac{d\mu}{dt}$, which is the spin rate of earth, is constant.

As is seen from figure 19, the $x_E\ y_E\ z_E$ system is obtained by rotating the $x_I\ y_I\ z_I$ system about the z-axis through the angle μ, thus

$$X_E = \begin{Bmatrix} x_E \\ y_E \\ z_E \end{Bmatrix} = \begin{bmatrix} \cos\mu & \sin\mu & 0 \\ -\sin\mu & \cos\mu & 0 \\ 0 & 0 & 1 \end{bmatrix} \begin{Bmatrix} x_I \\ y_I \\ z_I \end{Bmatrix} = T_\mu X_I \qquad (26)$$

where T_μ is the transform matrix shown.

The $x_M\, y_M\, z_M$ system is obtained by rotating the $x_E\, y_E\, z_E$ system, first about the x_E-axis by the tilt angle ζ, and then about the z_M-axis by the angle ν:

$$X_M = \begin{Bmatrix} x_M \\ y_M \\ z_M \end{Bmatrix} = \begin{bmatrix} \cos\nu & -\sin\nu & 0 \\ \sin\nu & \cos\nu & 0 \\ 0 & 0 & 1 \end{bmatrix} \begin{bmatrix} 1 & 0 & 0 \\ 0 & \cos\zeta & \sin\zeta \\ 0 & -\sin\zeta & \cos\zeta \end{bmatrix} \begin{Bmatrix} x_E \\ y_E \\ z_E \end{Bmatrix}$$

$$= T_\nu\, T_\zeta\, X_E \qquad (27)$$

Equations (26) and (27) yield

$$X_M = T_\nu\, T_\zeta\, T_\mu\, X_I \qquad (28)$$

The components of the vector in the inertial coordinate system are given in terms of the components in the geomagnetic coordinate system by solving equation (28) for X_I. The inverse of the orthogonal transformation $(T_\nu\, T_\zeta\, T_\mu)$ is obtained by reversing the rotations and their order, hence

$$X_I = T_{-\mu}\, T_{-\zeta}\, T_{-\nu}\, X_M \qquad (29)$$

The following approximations are now made:

1. The earth rotates a negligible amount during one orbital period of the satellite.

2. The summation of angular impulses over one day may be approximated by integration.

3. The satellite spin vector does not change significantly in one day.

The first two approximations are allowed by the relatively small variation in the geomagnetic inclination of the orbit i_M, and the corresponding small variations of the matrix elements of $A_{(i_M)}$, during a satellite orbital period. Typically, a near-earth satellite orbits the earth about 15 times per day, so that the earth rotates about 24° per orbit, and the geomagnetic inclination changes at the most by about 6° per orbit. The third approximation was discussed and used in chapter VII, section A, and is repeated because of its use here. Any errors introduced by these assumptions would be expected to average out over a time lapse of several days.

Equation (15) gives the average torque on the satellite as it moves in a fixed orbit through a fixed magnetic field. However, relative to the geomagnetic coordinate system, which now turns, the satellite does not move in a plane. These approximations permit the use of equation (15) to express the torque in terms of the osculating plane in the geomagnetic coordinate system; it is necessary only to reference the vectors to the geomagnetic coordinate system:

$$T_\nu\, T_\zeta\, T_\mu \left\{\overline{M}_{av}\right\}_I = -\frac{Ks^2}{p^6} A(i_M)\, T_\nu\, T_\zeta\, T_\mu \left\{\omega\right\}_I \qquad (30)$$

whence

$$\left\{M_{av}\right\}_I = -\frac{Ks^2}{p^6} B_{(i_I,\mu)} \left\{\omega\right\}_I \qquad (31)$$

where $B(i_I,\mu)$ is given by

$$B(i_I,\mu) = T_{-\mu}\, T_{-\zeta}\, T_{-\nu}\, A\, i_M\, T_{\nu}\, T_{\zeta}\, T_{\mu} \tag{32}$$

and is seen to be simply the similarity transform of $A(i_M)$ from the geomagnetic coordinate system to the inertial coordinate system. The average daily torque is thus written as

$$\langle M_{eddy} \rangle_I = -\frac{Ks^2}{p^6} \frac{1}{2\pi} \oint B(i_I,\mu) \langle \omega \rangle_I \, d\mu$$

$$= -\frac{Ks^2}{p^6} B(i_I) \langle \omega \rangle_I \tag{33}$$

The matrix $B(i_I)$, which now takes the place of $A(i_M)$, is

$$B\, i_I = \frac{1}{2\pi} \oint B(i_I,\mu) \, d\mu \tag{34}$$

The integration indicated in equation (34) was accomplished numerically. The matrix $B(i_I,\mu)$ being a similarity transform of $A(i_M)$, which is symmetric, is also symmetric, hence its integral, $B(i_I)$, is symmetric. The b_{12} and b_{13} (hence b_{21} and b_{31}, by symmetry) terms are found to be only a fraction of a percent of the larger terms in the matrix, and may be considered to be negligible. The remaining, predominant, matrix elements b_{11}, b_{22}, b_{33}, and b_{23} (= b_{32}) are plotted as functions of i_I, the inclination of the orbit plane to the equator, in figure 20.

Equation (33) can be used to calculate the daily-average torque due to eddy currents on a spinning satellite. The time history of the effect of this torque can be determined by the same analysis as used in the previous section; equations (15) through (25) are immediately applicable

when the elements of $B(i_I)$ are substituted for the elements of $A(i_M)$. The eigenvalues of $B(i_I)$, Λ_1, Λ_2, and Λ_3 are shown in figure 21 as a function of i_I, and the angle χ_I between the eigenvectors of $B(i_I)$ and the space-fixed coordinate axes is shown in figure 22, also as a function of i_I.

C. Numerical Example

In order to illustrate the application of the theory developed in this thesis, the spin decay of a typical satellite is calculated. For the calculations, the following numbers are used:

$$I = 2.0 \times 10^7 \text{ gm-cm}^2$$

$$K = 50 \text{ dyne-cm-sec/gauss}^2$$

$$p = 1.15 R_e$$

$$i_I = 52^\circ$$

$$s = 0.3131$$

$$\text{Argument of perigee} = 142.3^\circ$$

The spin vector is considered to be initially tangent to the orbit at the perigee.

The initial spin vector, expressed in the space fixed coordinate system is thus

$$\bar{\omega}_0 = \omega_0 \begin{Bmatrix} \sin 142.3^\circ \\ -\cos 142.3^\circ \cos 52^\circ \\ -\cos 142.3^\circ \sin 52^\circ \end{Bmatrix} = \omega_0 \begin{Bmatrix} 0.612 \\ 0.487 \\ 0.624 \end{Bmatrix}$$

It is seen from figure 9 that for $i_I = 52^\circ$, $\chi_I = 46^\circ$, so that by equation (25)

$$\begin{Bmatrix} a_1 \\ a_2 \\ a_3 \end{Bmatrix} = \begin{bmatrix} 1 & 0 & 0 \\ 0 & \cos 46^\circ & \sin 46^\circ \\ 0 & -\sin 46^\circ & \cos 46^\circ \end{bmatrix} \bar{\omega}_0 = \omega_0 \begin{Bmatrix} 0.612 \\ .788 \\ .083 \end{Bmatrix}$$

From equation (24)

$$\tau = \frac{50}{2.0 \times 10^7} \frac{.313^2}{1.15^6} t = 1.06 \times 10^{-7}\, t \text{ (sec)}$$

$$= 0.916 \times 10^{-2}\, t \text{ (days)}$$

The eigenvalues for $i_I = 52^\circ$ are shown by figure 8 to be

$$\lambda_1 = 1.26$$

$$\lambda_2 = 1.54$$

$$\lambda_3 = 1.14$$

The equation for the spin vector, equation (23), thus becomes

$$\bar{\omega}/\omega_0 = 0.612 \begin{Bmatrix} 1 \\ 0 \\ 0 \end{Bmatrix} e^{-.0115t} + 0.788 \begin{Bmatrix} 0 \\ 0.695 \\ .719 \end{Bmatrix} e^{-.0141t} + 0.083 \begin{Bmatrix} 0 \\ -.719 \\ .695 \end{Bmatrix} e^{-.0104t}$$

$$= \begin{Bmatrix} 0.612 \\ 0 \\ 0 \end{Bmatrix} e^{-.0115t} + \begin{Bmatrix} 0 \\ 0.548 \\ .567 \end{Bmatrix} e^{-.0141t} + \begin{Bmatrix} 0 \\ -.060 \\ .058 \end{Bmatrix} e^{-.0104t}$$

The time history of the spin vector is thus given explicitly by this equation.

VIII. CONCLUSIONS

A study has been made of the torque due to eddy currents induced by the geomagnetic field on a spinning satellite.

In the first part of the study, an analysis was made of the eddy currents induced by a known applied magnetic field on the following spinning shapes:

1. Thin-wall symmetrically spinning cylinder
2. Thick-wall symmetrically spinning cylinder
3. Thin-wall tumbling cylinder
4. Thin-wall cone and cone frustum
5. Joined thin-wall cone frustums, and
6. General thin-wall body of revolution.

From the current expressions, the torques are calculated. Figures showing the variation of torque with fineness ratio and thickness ratio are presented for thin- and thick-wall cylinders.

In the second part of the study, an analysis was made of the torque due to induced eddy currents which act on the spinning satellite while in a near-earth orbit. The earth's magnetic field was assumed to be that of a space-fixed dipole, and the equation for the average torque was derived. This analysis showed the variation of the torque with the orbit parameters. The time history of the spin vector subject to this torque has been investigated. It was found that, for the general case, the spin vector can be resolved into three orthogonal components which are exponentially damped, but at three different rates.

The effect of the tilt of the geomagnetic dipole axis on the torque was next considered, and the resulting spin history of the satellite determined. The results of this analysis were found to be qualitatively similar to those obtained from the preceding analysis, which did not consider the tilt.

Quantitative results of the analyses are presented in graphical form.

IX. ACKNOWLEDGMENTS

The author wishes to express his appreciation to the National Aeronautics and Space Administration for the permission to use material in this thesis that was obtained from research conducted at the Langley Research Center.

In particular, the author wishes to thank for her help in preparing the final figures.

He also wishes to thank of the Aerospace Engineering Department for his advice and assistance in preparing this thesis.

X. REFERENCES

1. Rosenstock, Herbert B.: The Effect of the Earth's Magnetic Field on the Spin of the Satellite. Astronautica Acta, Vol. III, Fasc. 3, 1957, pp. 215-221.

2. Wilson, Raymond H., Jr.: Magnetic Damping of Rotation of Satellite $1958\beta_2$ (Vanguard I). Science, Vol. 130, No. 3378, Sept. 25, 1959, pp. 791-793.

3. Wilson, Raymond H., Jr.: Geomagnetic Rotational Retardation of Satellite 1959α (Vanguard II). Science, Vol. 131, No. 3395, Jan. 22, 1960, pp. 223-225.

4. Zonov, Yu. V.: On the Problem of Interaction Between a Satellite and the Earth's Magnetic Field. NASA TT F-37, 1960.

5. Vinti, John P.: Theory of the Spin of a Conducting Satellite in the Magnetic Field of the Earth. Rep. No. 1020, Ballistic Res. Labs., Aberdeen Proving Ground, July 1957.

6. Smythe, William R.: Static and Dynamic Electricity. McGraw-Hill Book Co., Inc. 1939.

7. Sanduleak, N.: A Generalized Approach to the Magnetic Damping of the Spin of a Metallic Earth Satellite. Army Ballistic Missile Agency DG-TM-151-58. Oct. 1, 1958.

8. Thomson, William T., and Reiter, Gordon S.: Attitude Drift of Space Vehicles. Journal of the Astronautical Sciences, Vol. VII, No. 2, Summer, 1960.

The vita has been removed from the scanned document

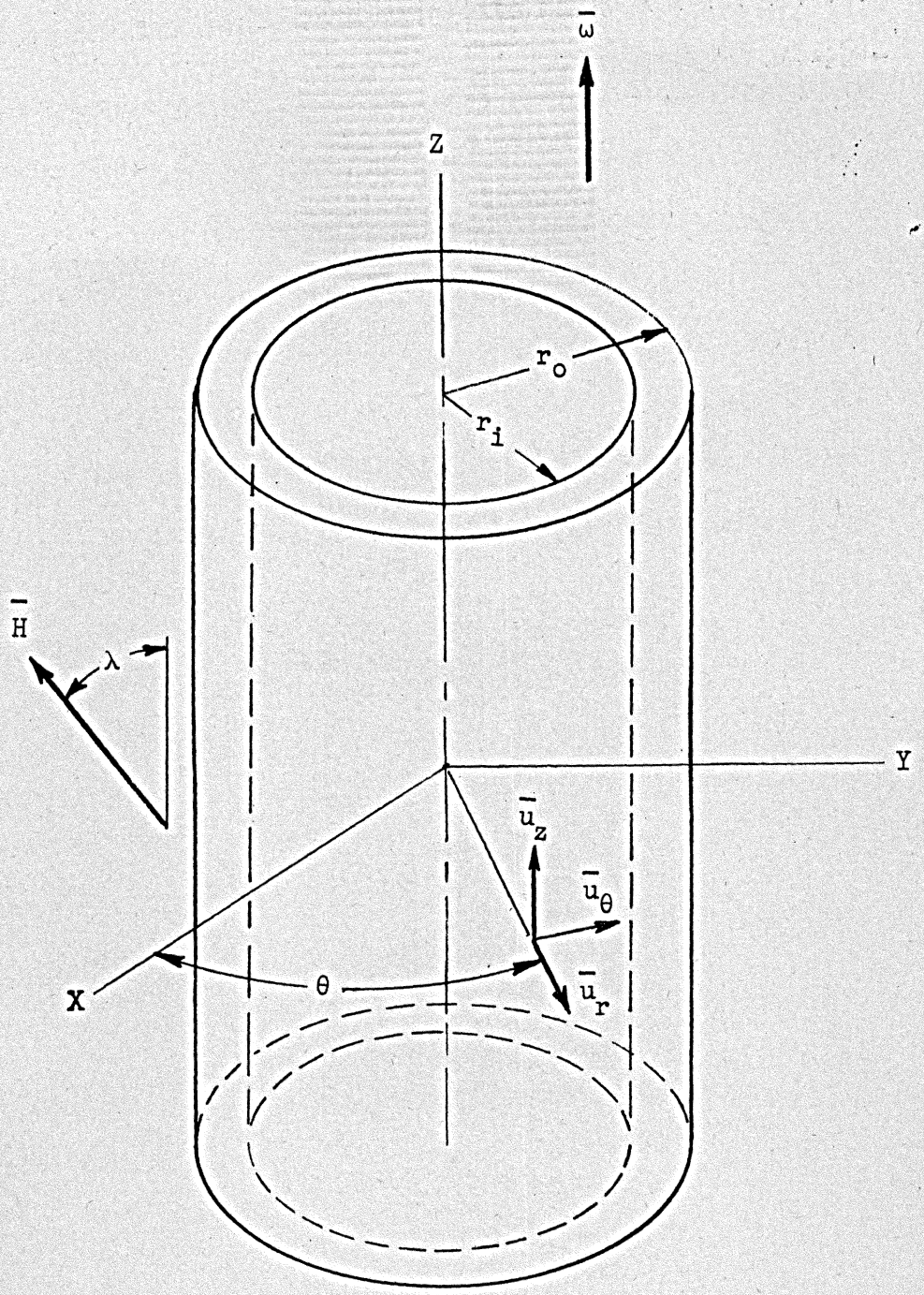

Figure 1.- Coordinate systems for symmetrically spinning cylinder.

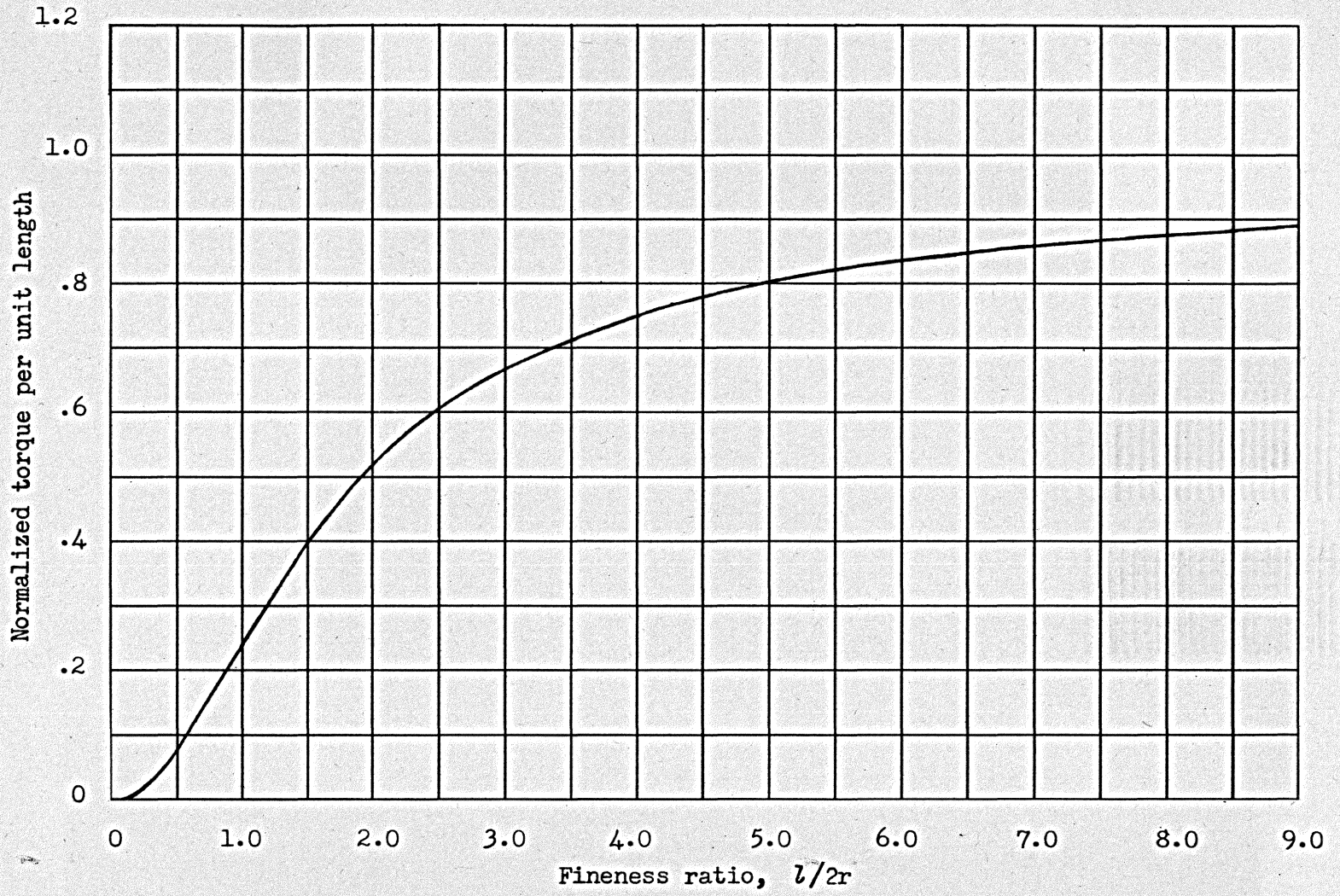

Figure 2.- Normalized torque per unit length as a function of fineness ratio for spinning thin-wall cylinder.

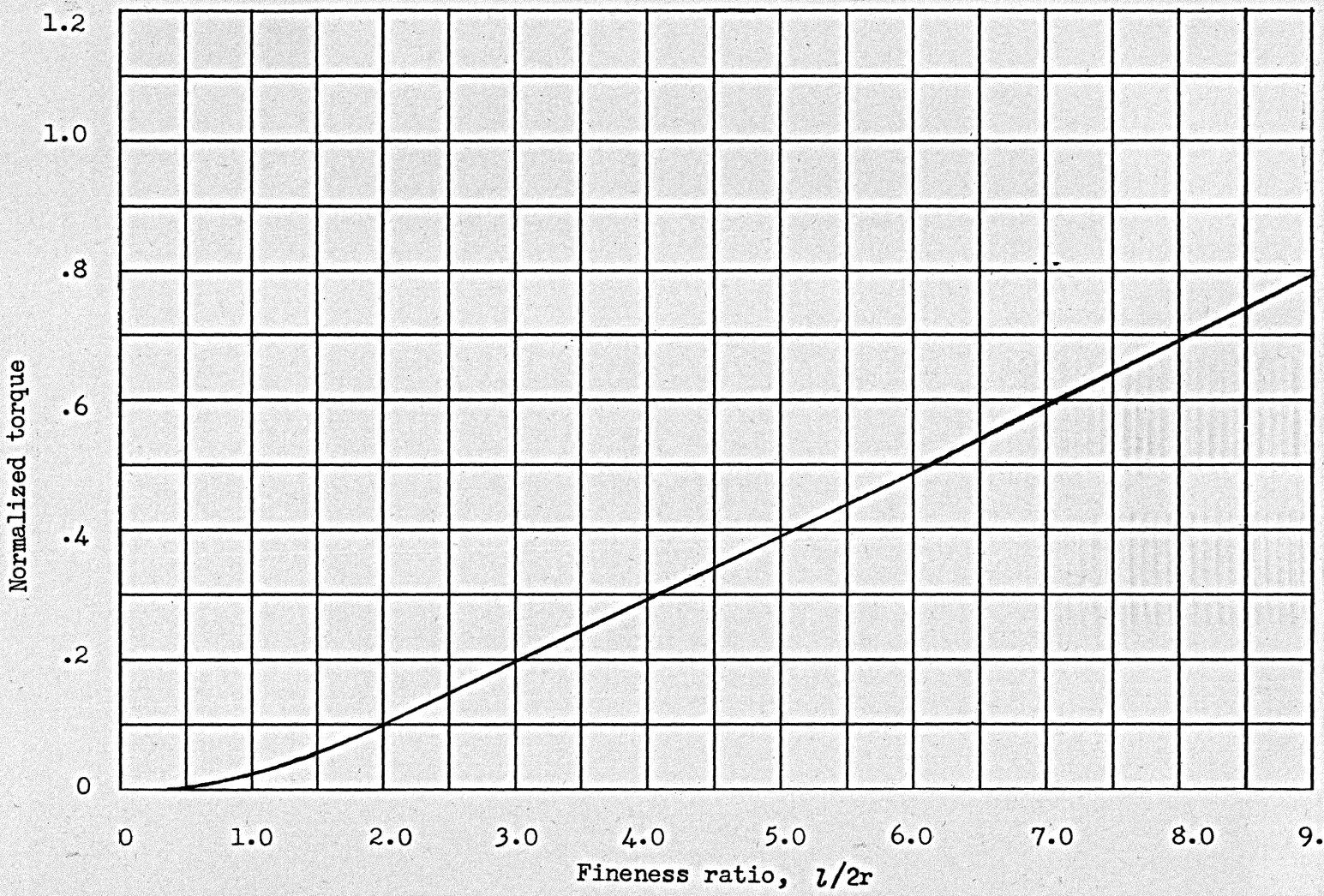

Figure 3.- Normalized torque as a function of fineness ratio for spinning thin-wall cylinder.

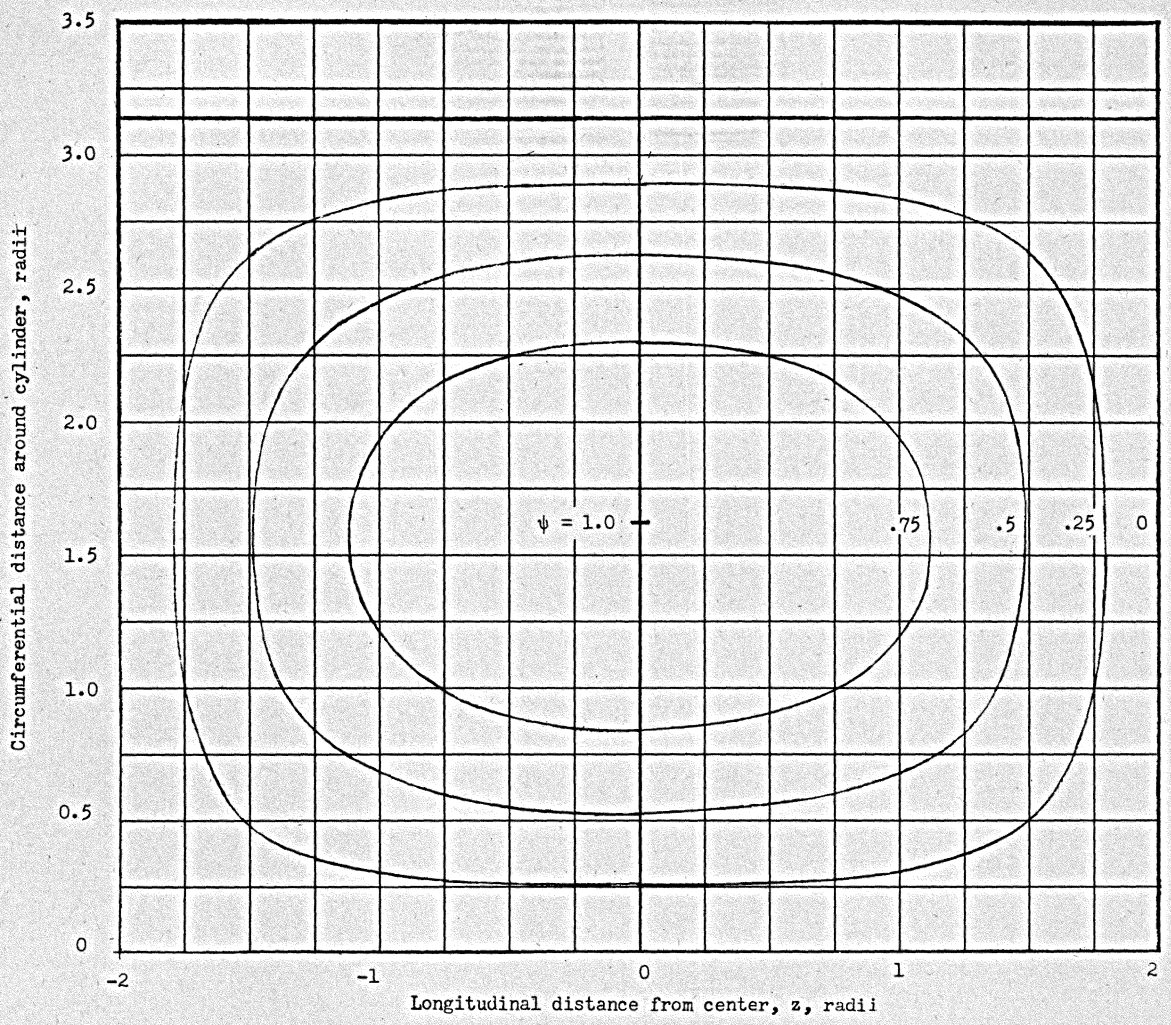

(a) Fineness ratio $\frac{l}{2r} = 2.$

Figure 4.- Current paths for spinning thin-wall cylinder.

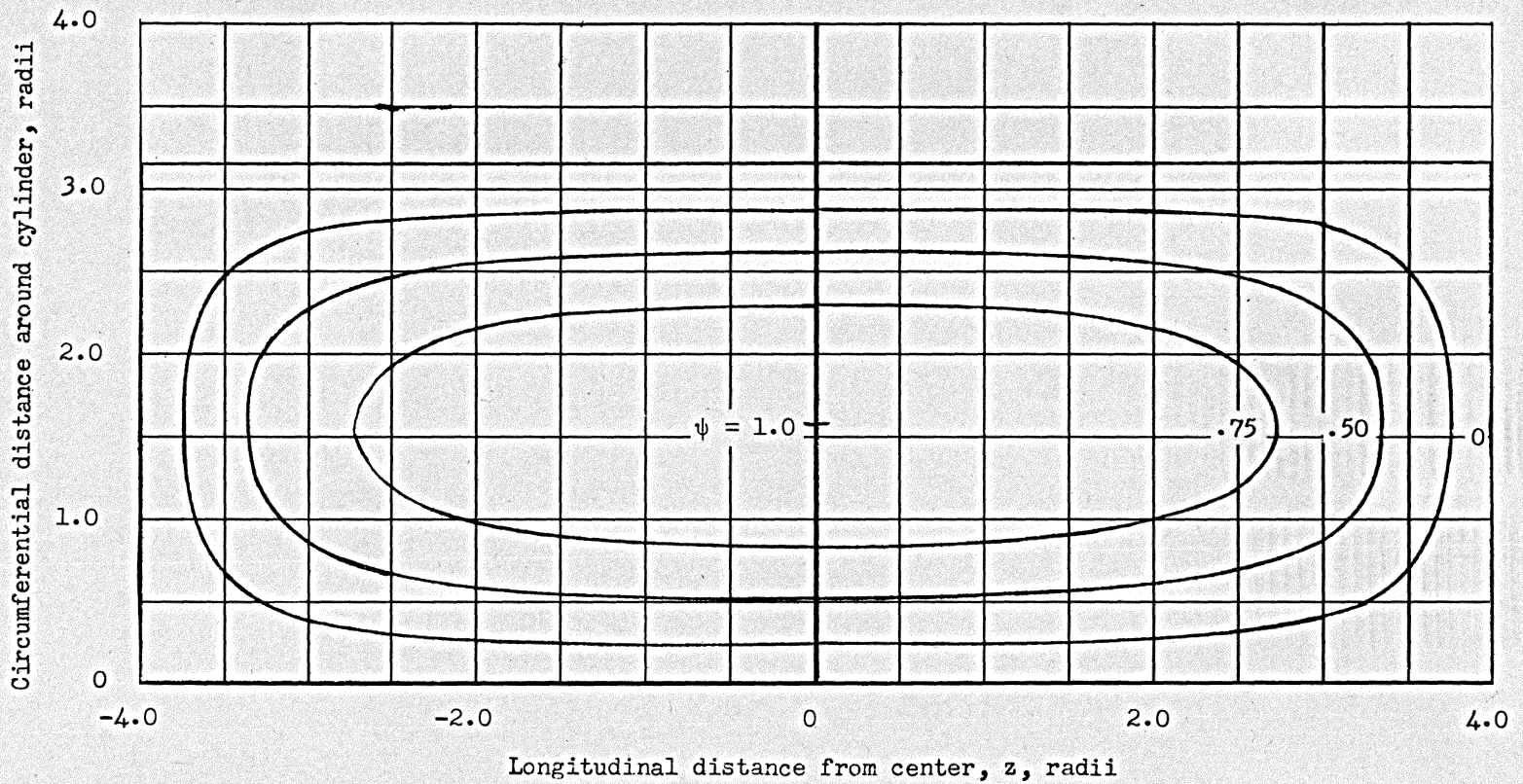

(b) Fineness ratio $\frac{l}{2r} = 4.$

Figure 4.- Continued.

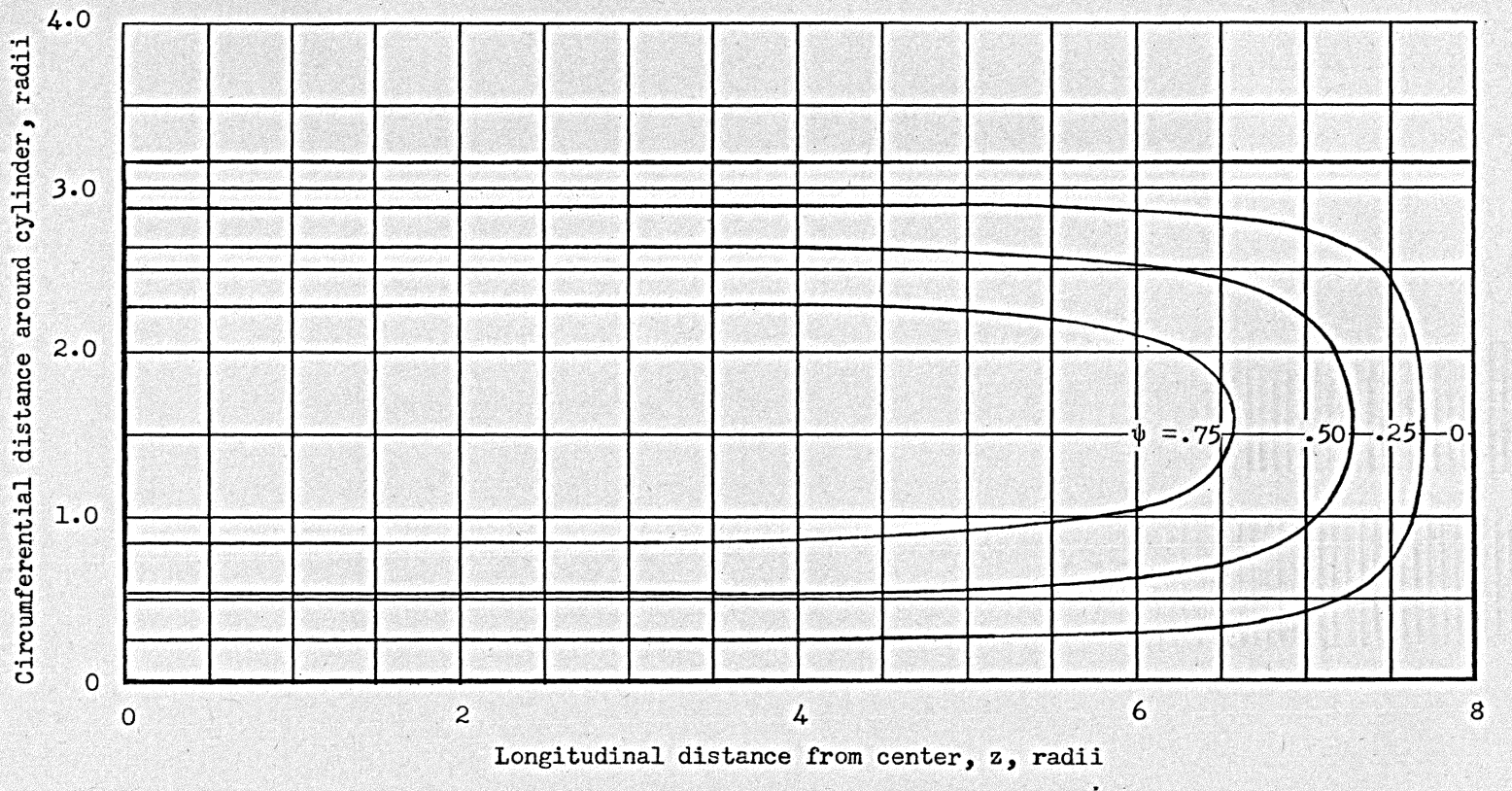

(c) Fineness ratio $\frac{l}{2r} = 8.$

Figure 4.- Concluded.

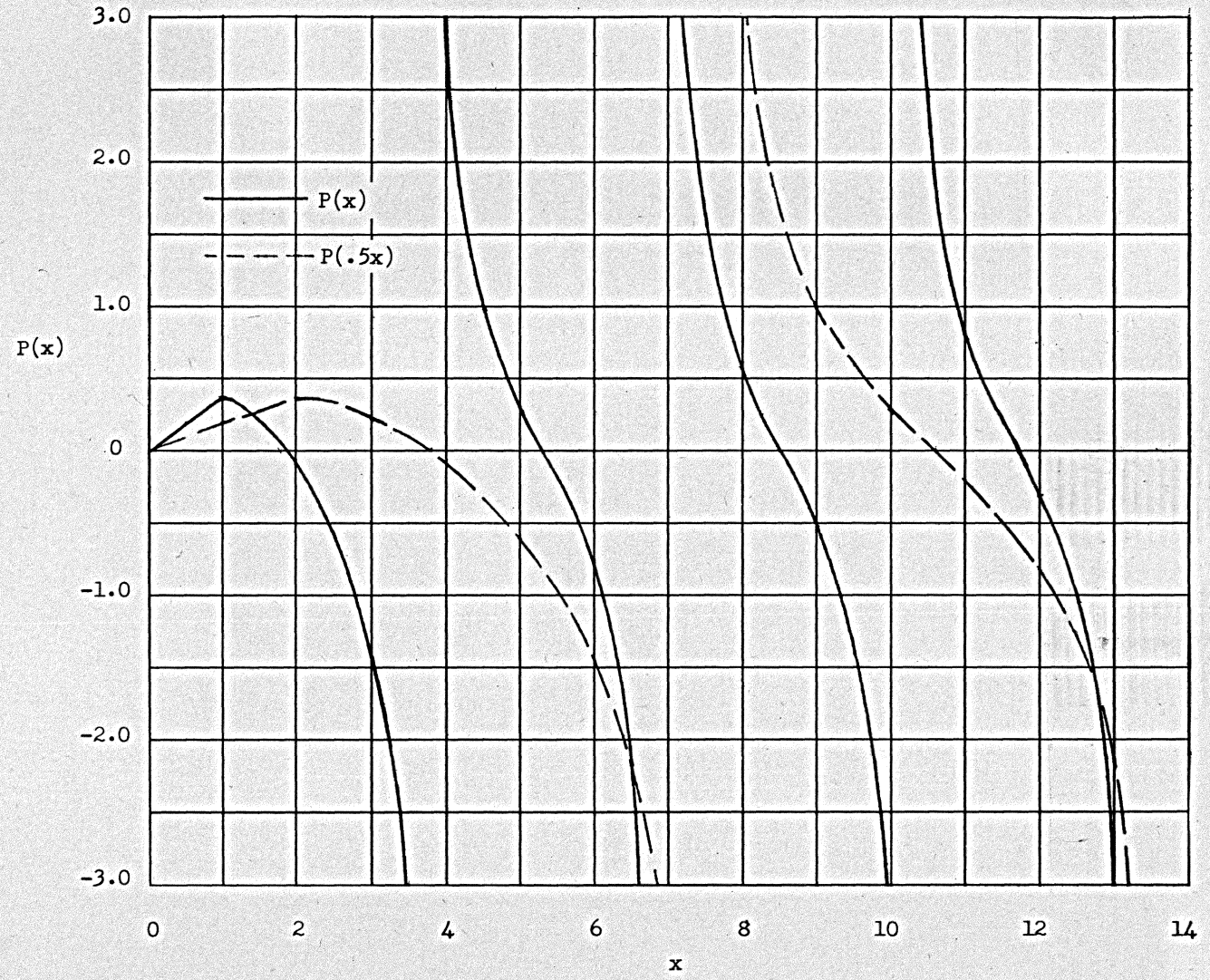

Figure 5.- Plot for graphical determination of eigenvalues.

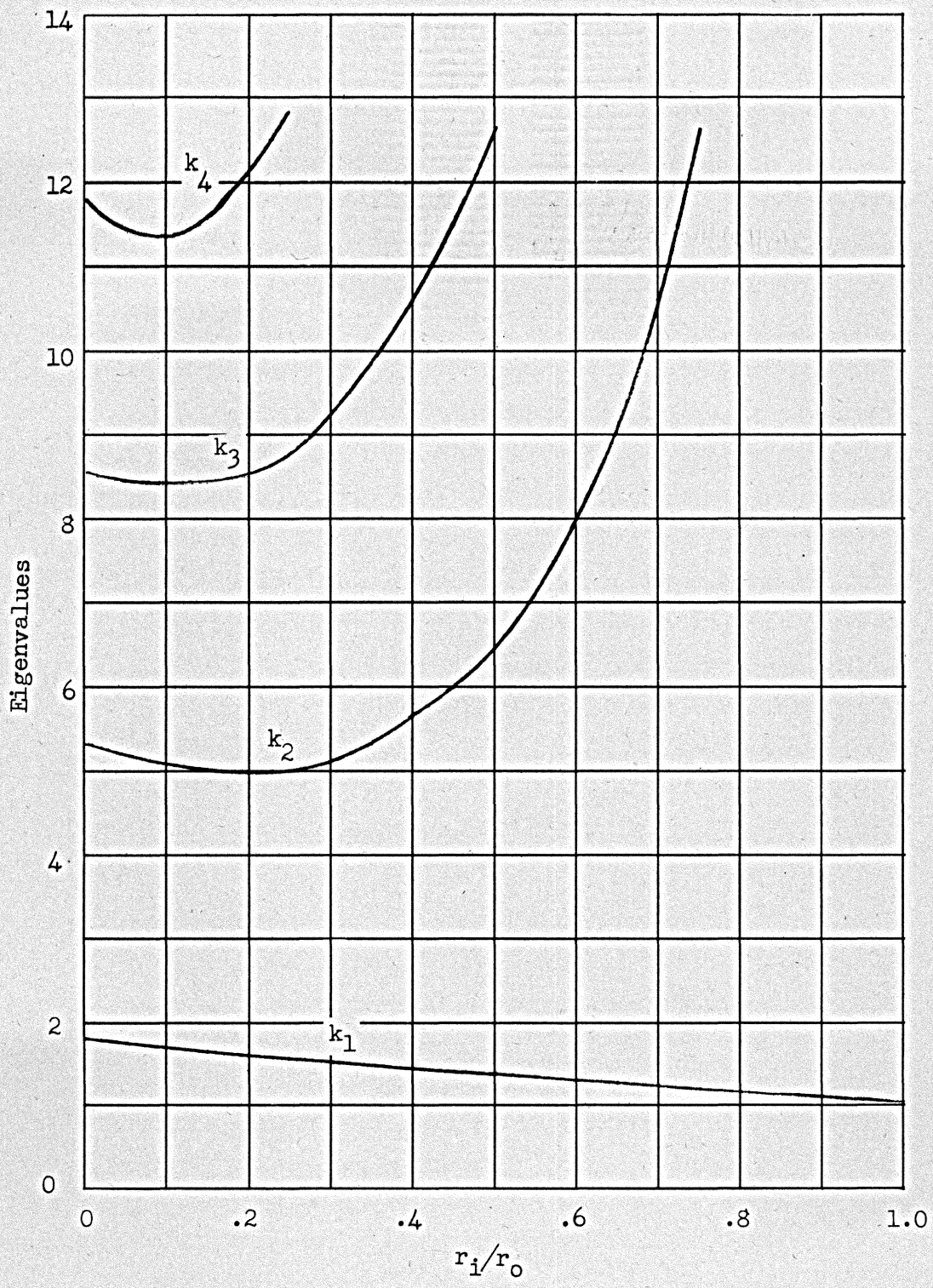

Figure 6.- Variation of eigenvalues with r_i/r_o.

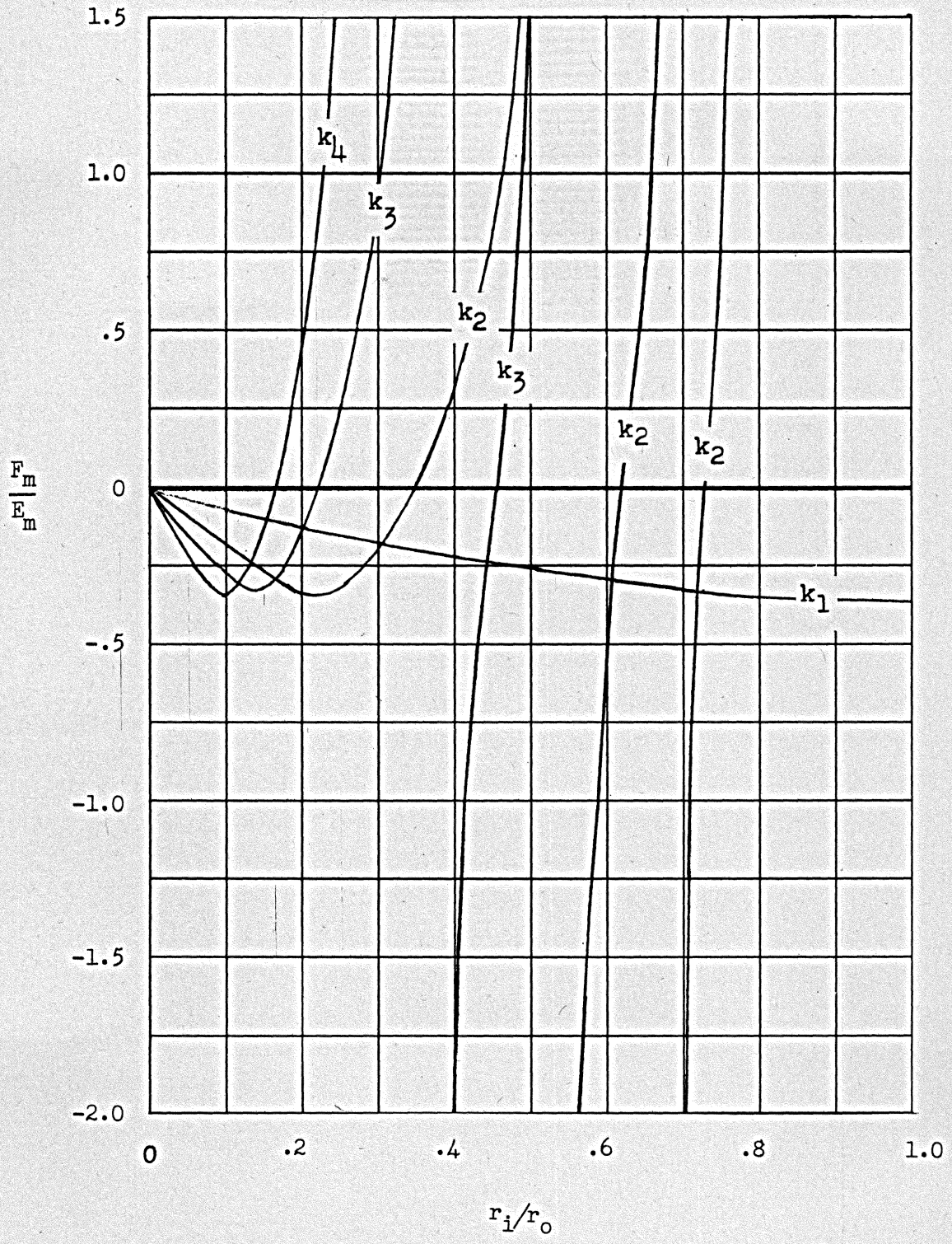

Figure 7.- Variation of F_m/E_m with r_i/r_o for different eigenvalues.

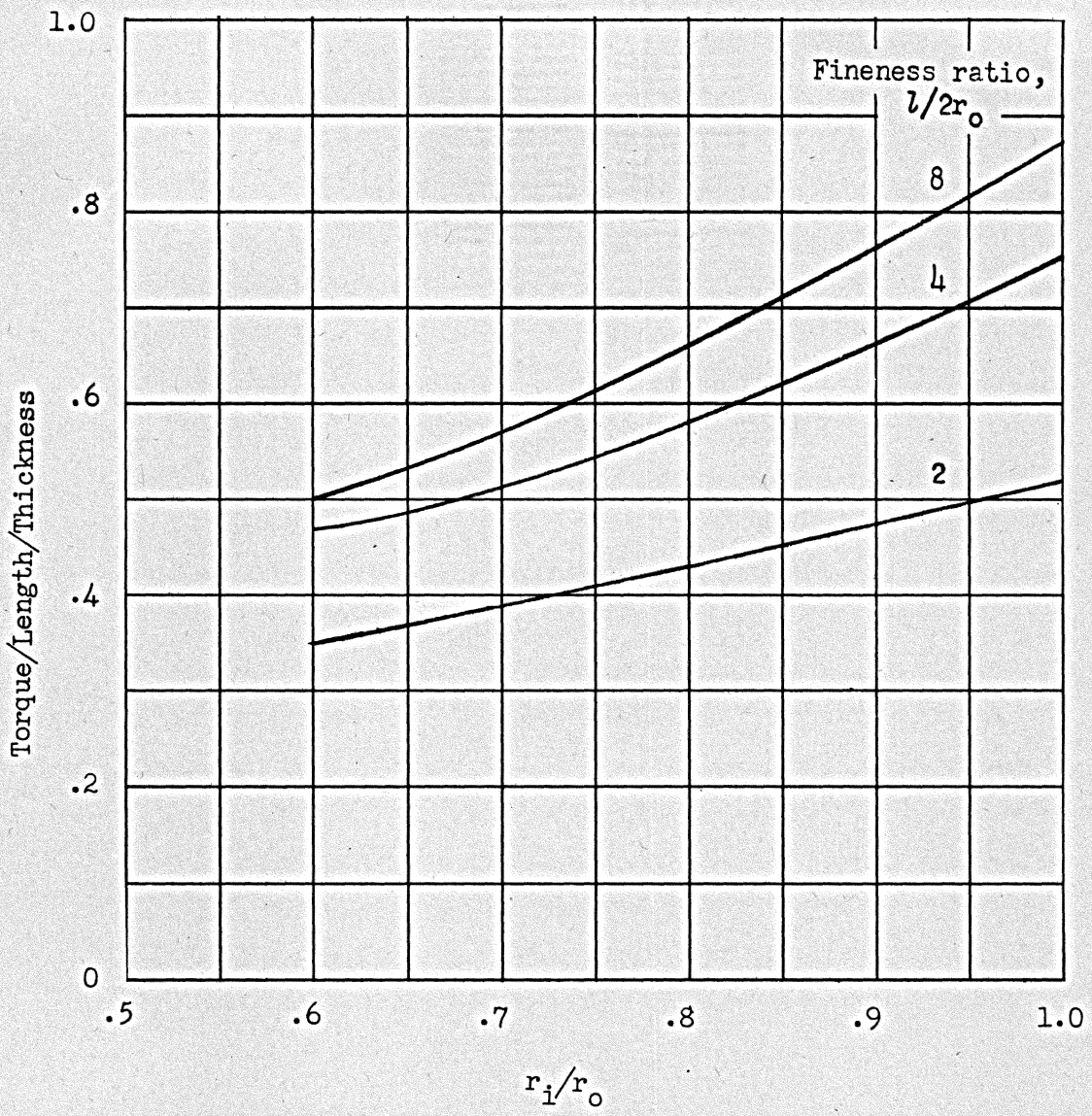

Figure 8.- Torque per unit length per unit thickness as a function of r_i/r_o for spinning thick-wall cylinder. The product $\sigma c^{-2} h^2 \omega r_o^4$ is taken to be unity.

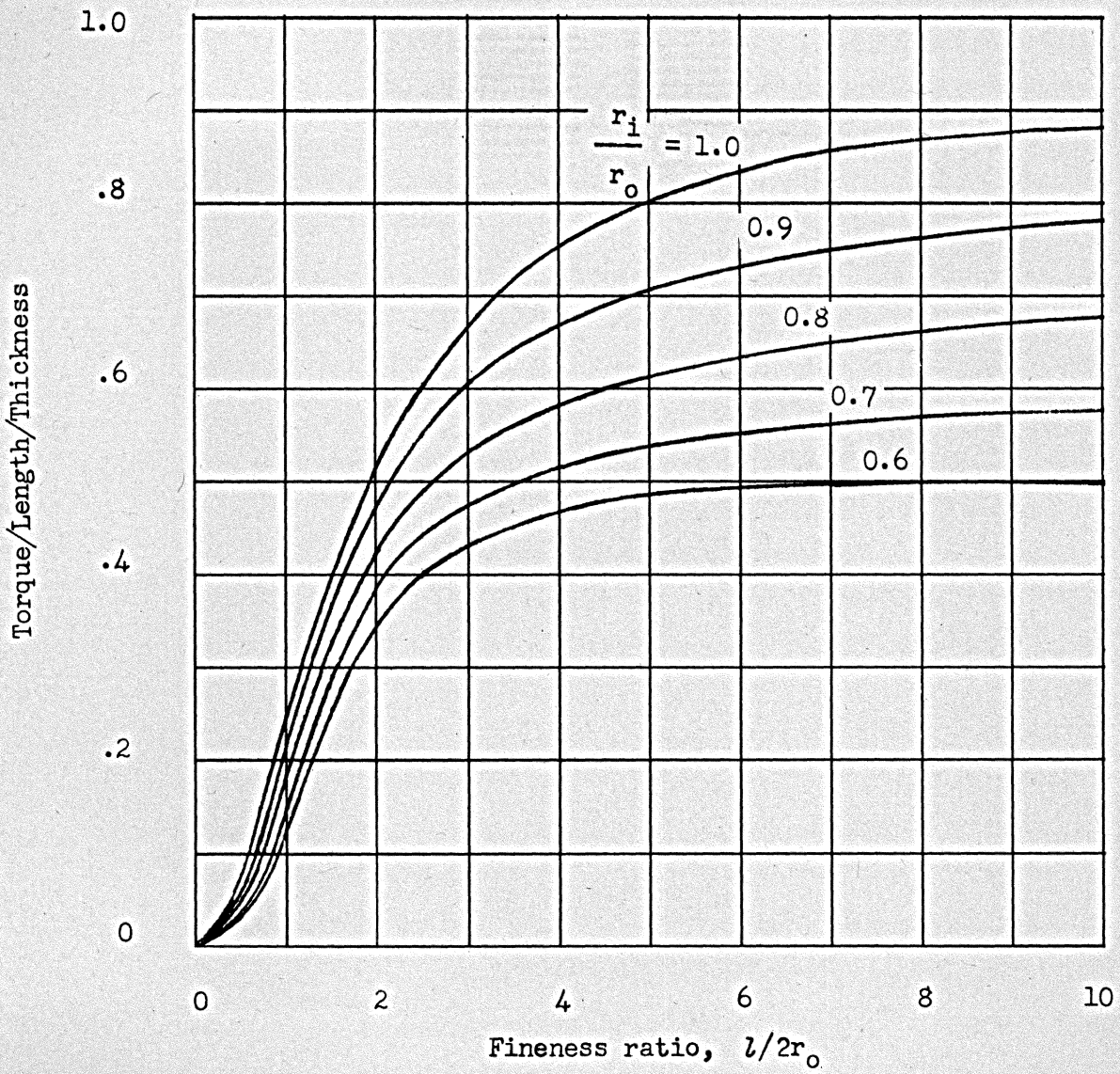

Figure 9.- Torque per unit length per unit thickness as a function of fineness ratio for spinning thick-wall cylinder. The product $\sigma c^{-2} h^2 \omega r_o$ is taken to be unity.

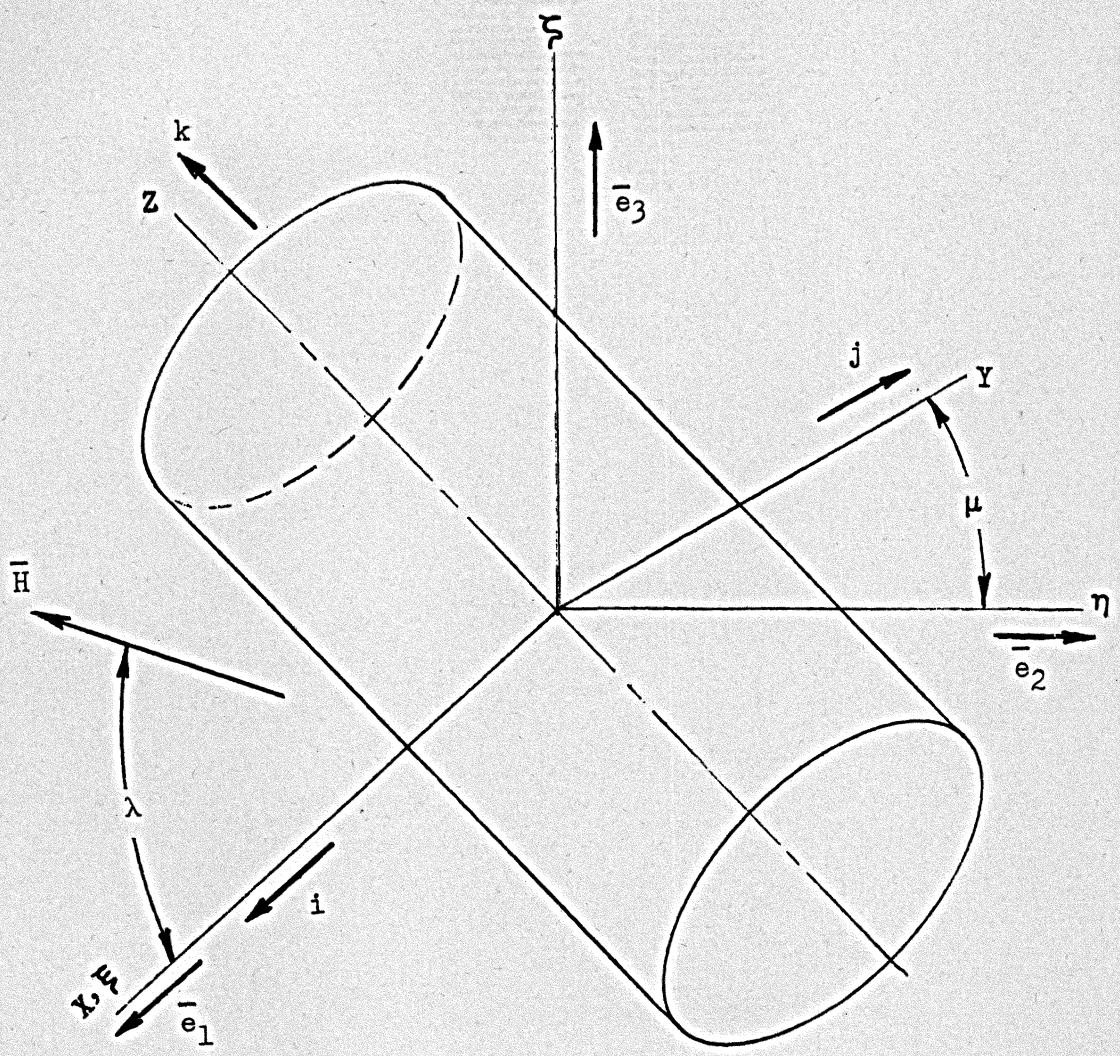

Figure 10.- Coordinate systems for tumbling cylinder.

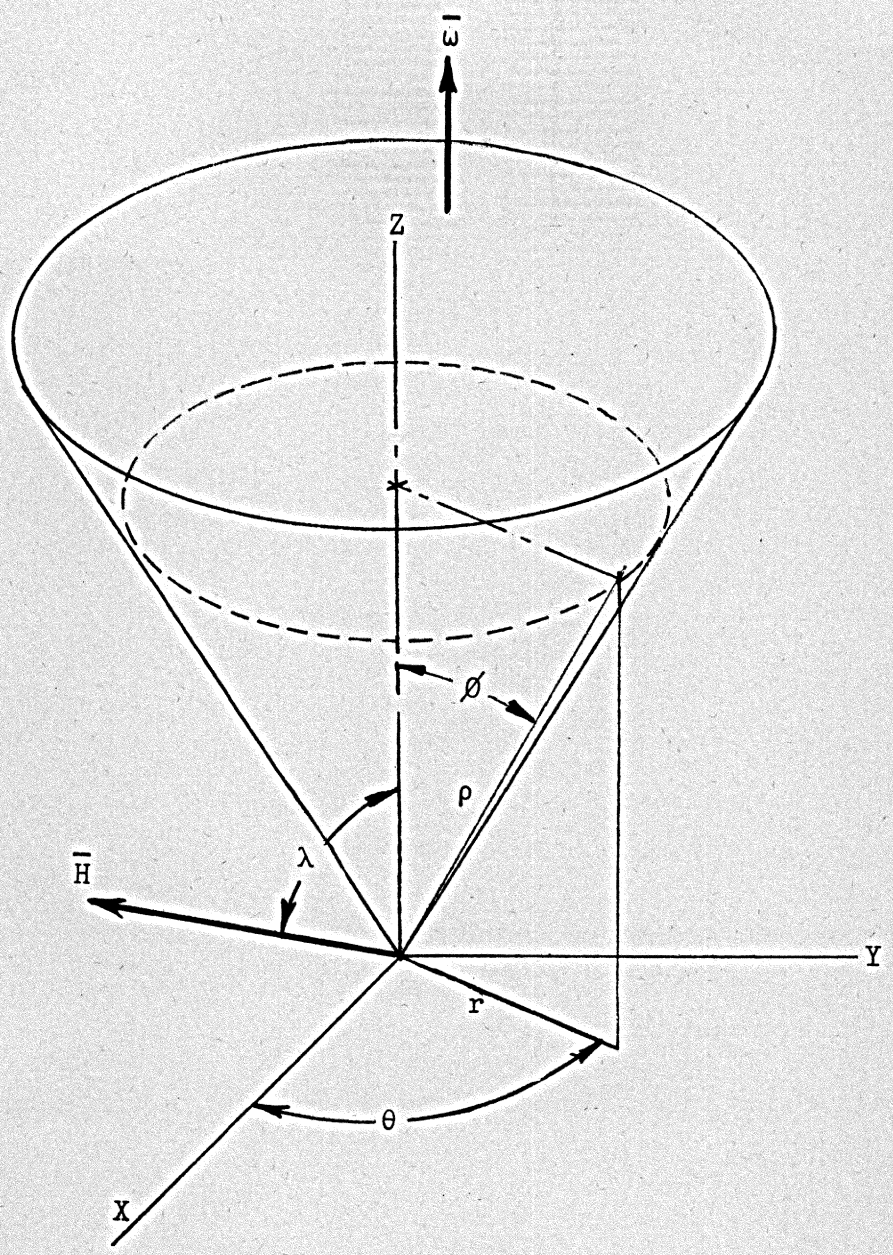

Figure 11.- Coordinate systems for cone.

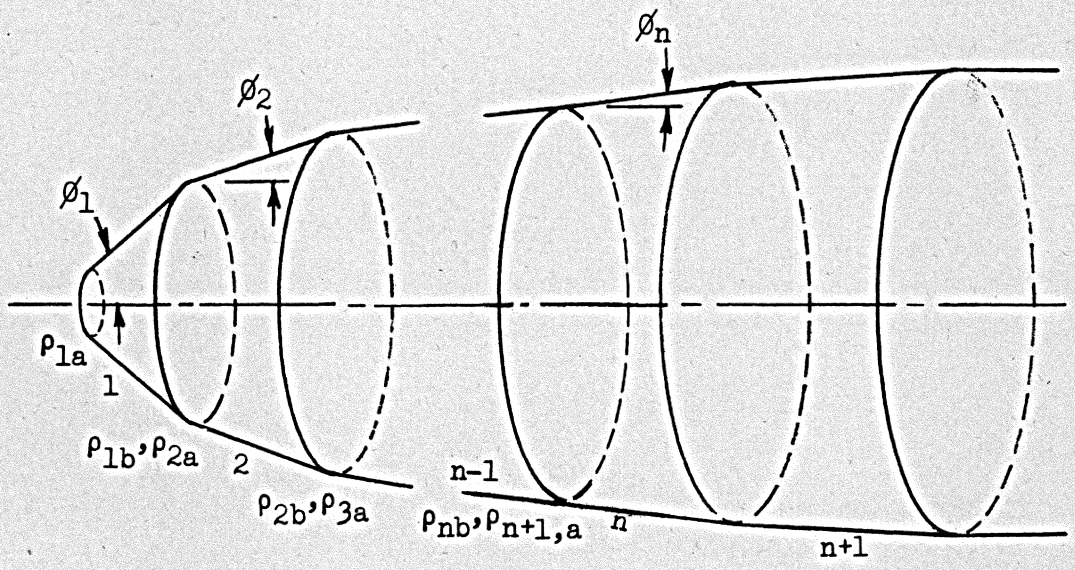

Figure 12.- Series of cone frustums.

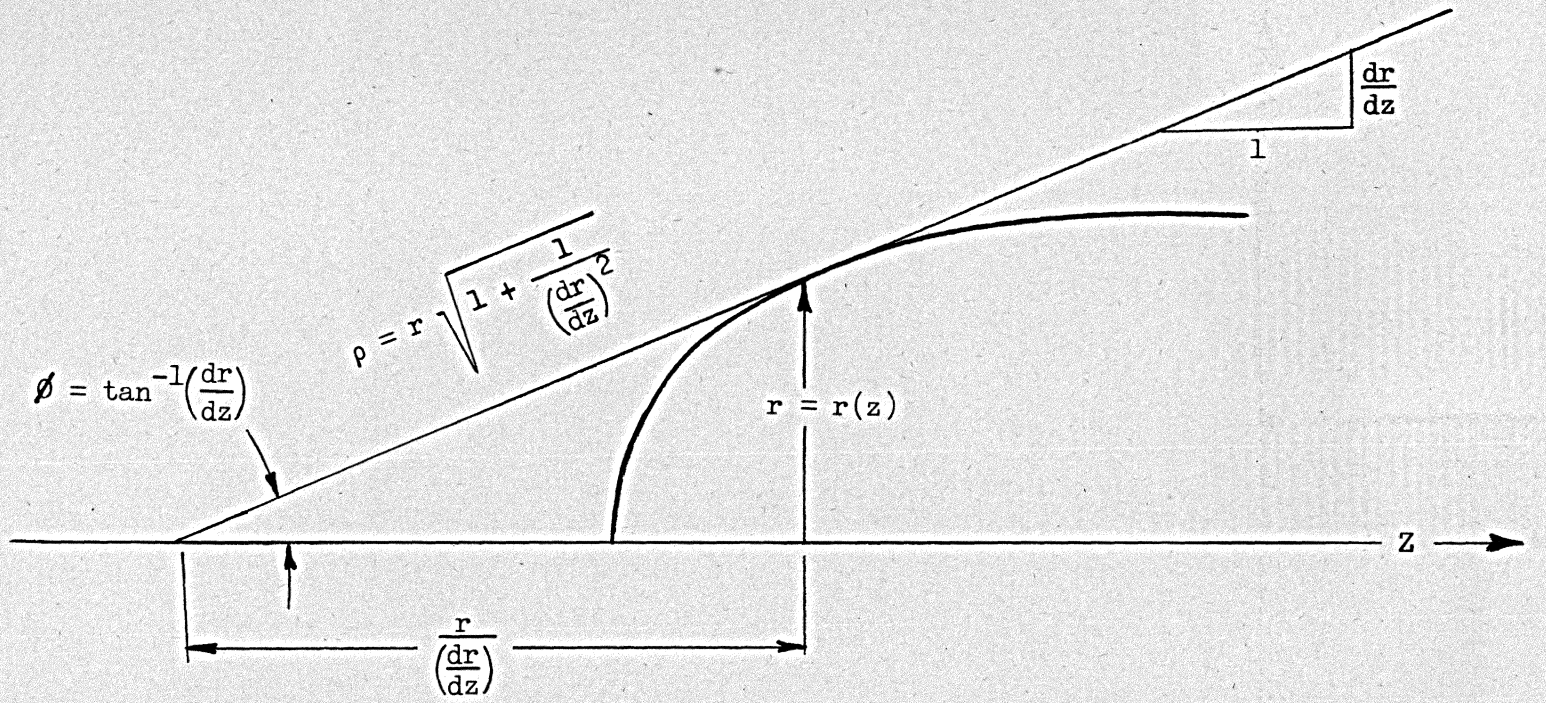

Figure 13.- Geometry of general body of revolution.

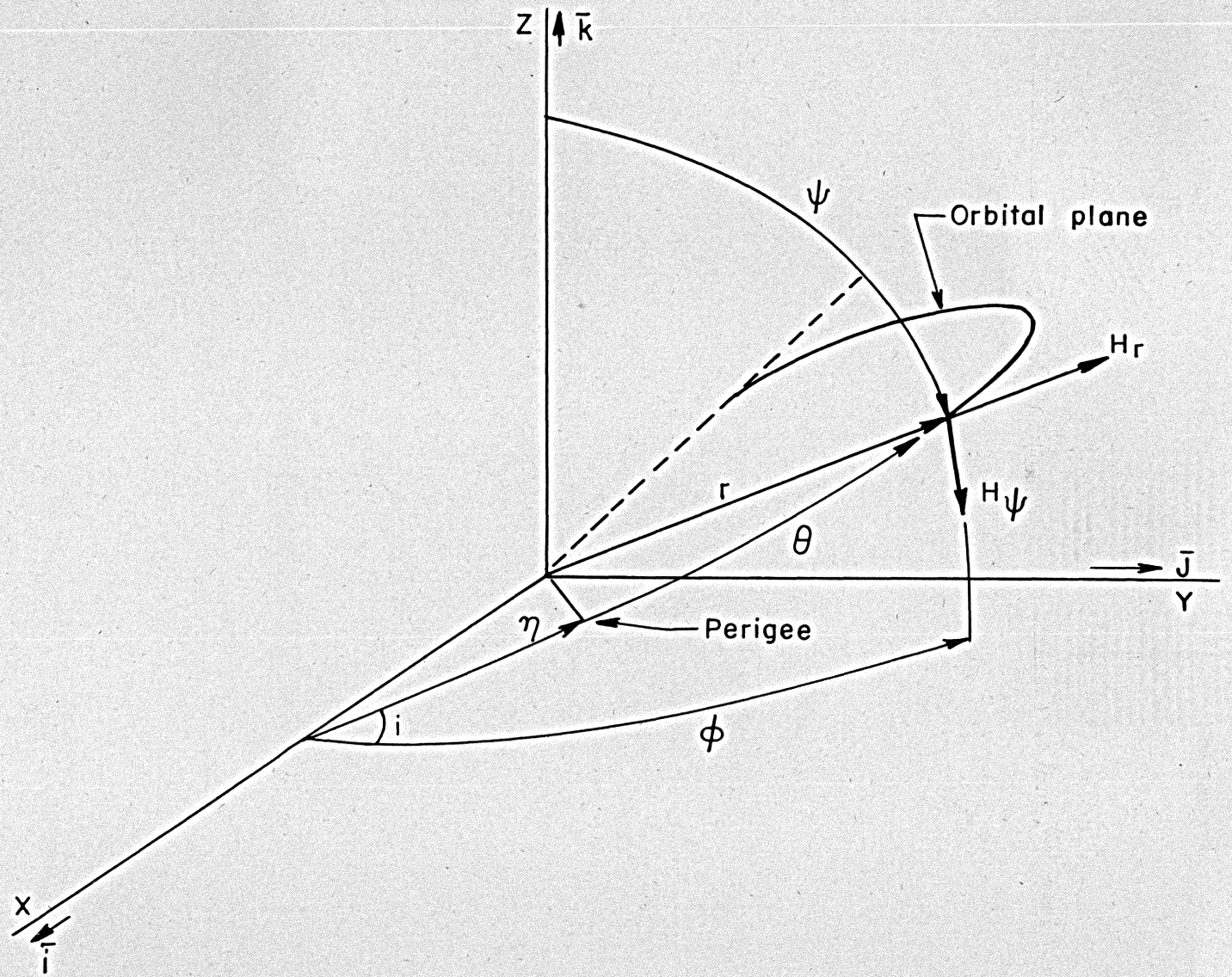

Figure 14.- Coordinate systems for noninclined dipole.

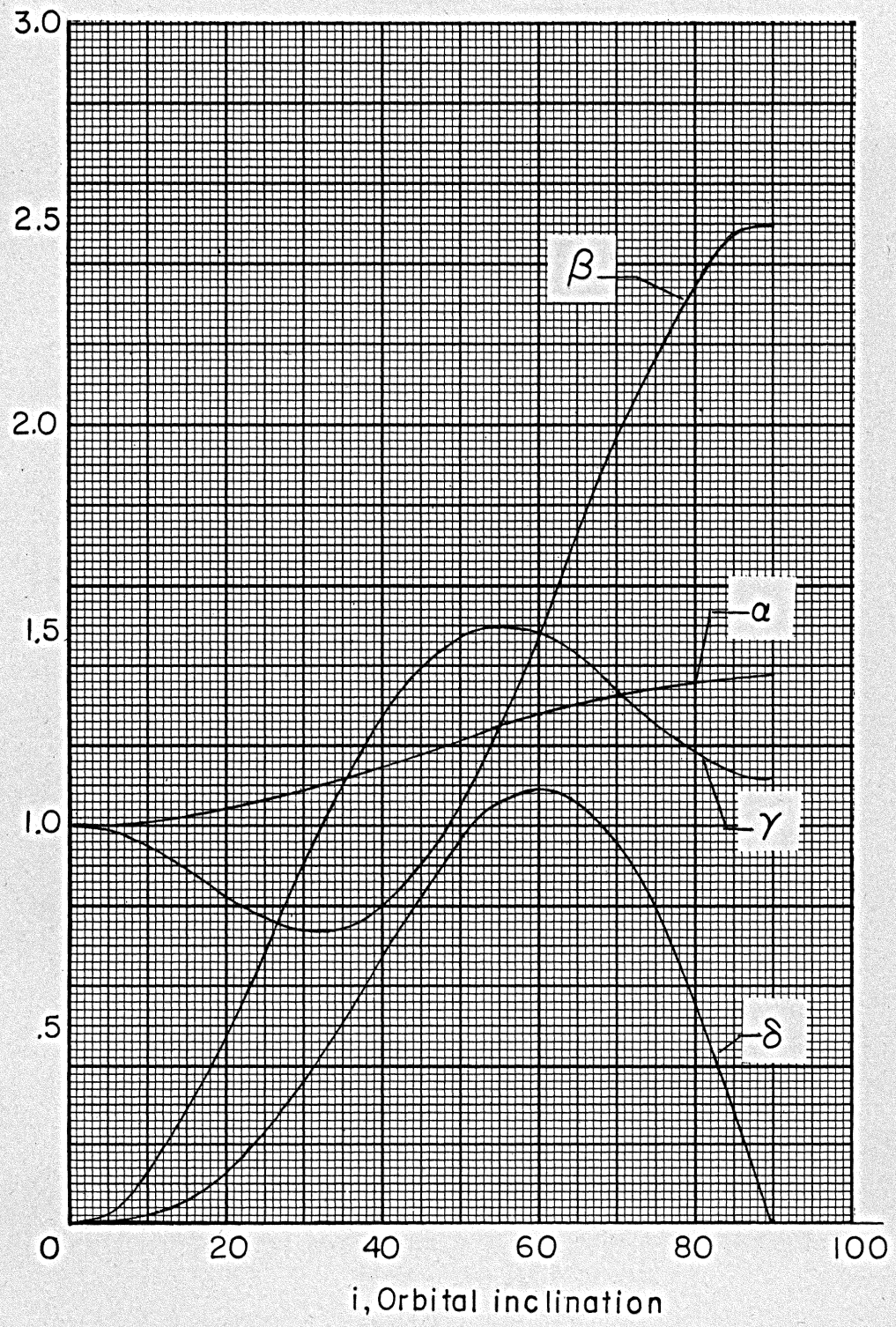

Figure 15.- Elements of A (i) matrix as a function of orbital inclination.

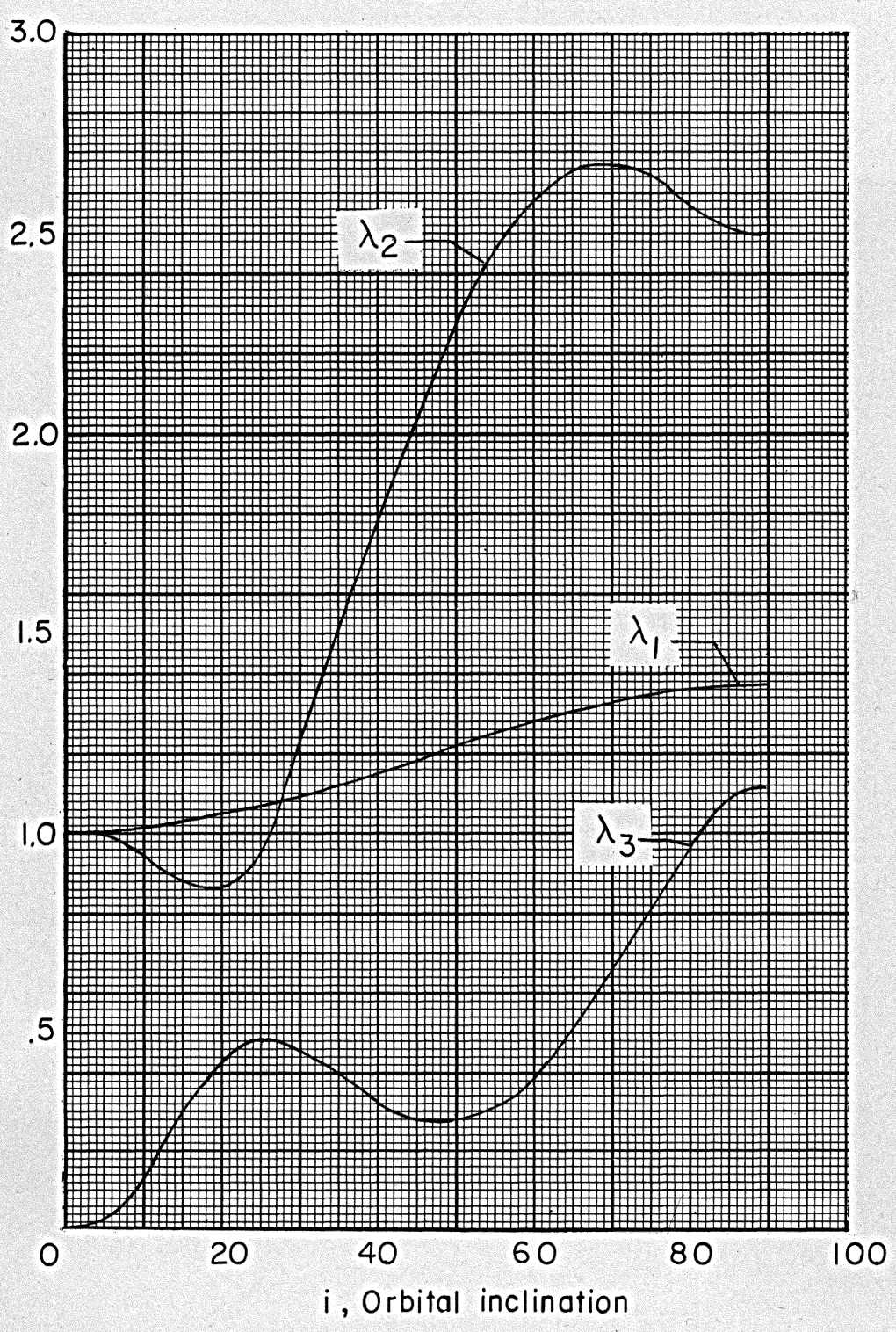

Figure 16.- Eigenvalues of A (i) matrix as a function of orbital inclination.

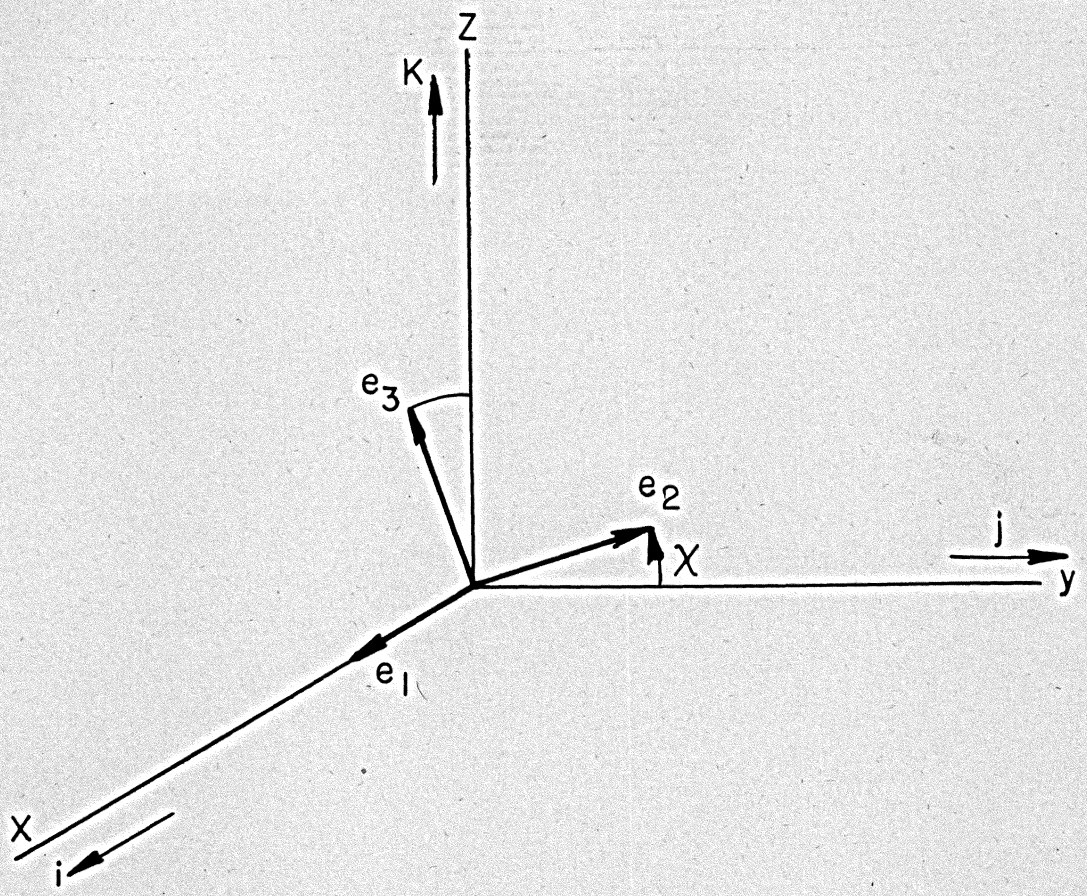

Figure 17.- Relation between coordinate systems and eigenvectors.

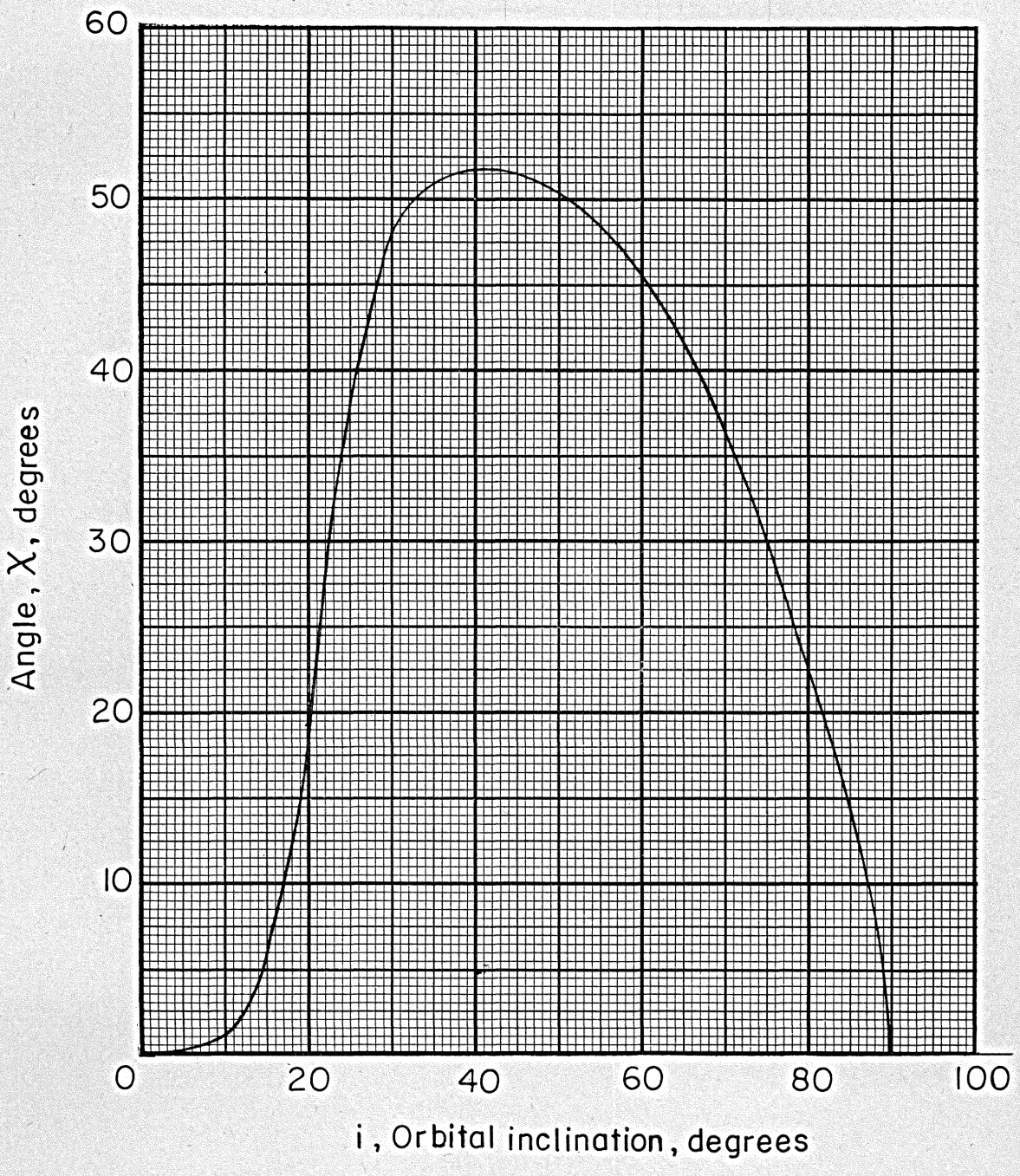

Figure 18.- Angle X, between eigenvectors and coordinate axes, as function of orbital inclination, i.

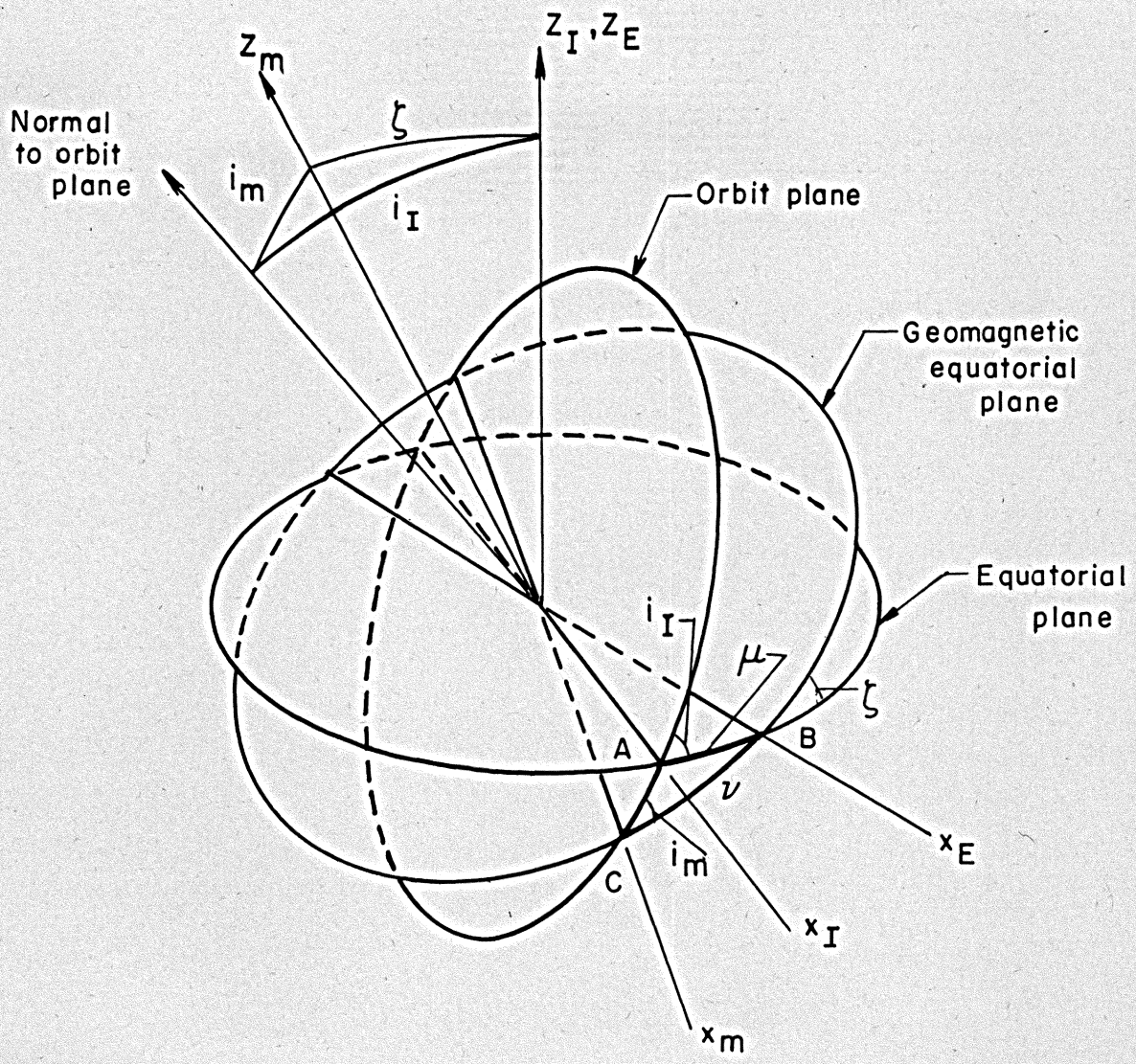

Figure 19.- Coordinate systems used for calculation of torques due to tilted dipole.

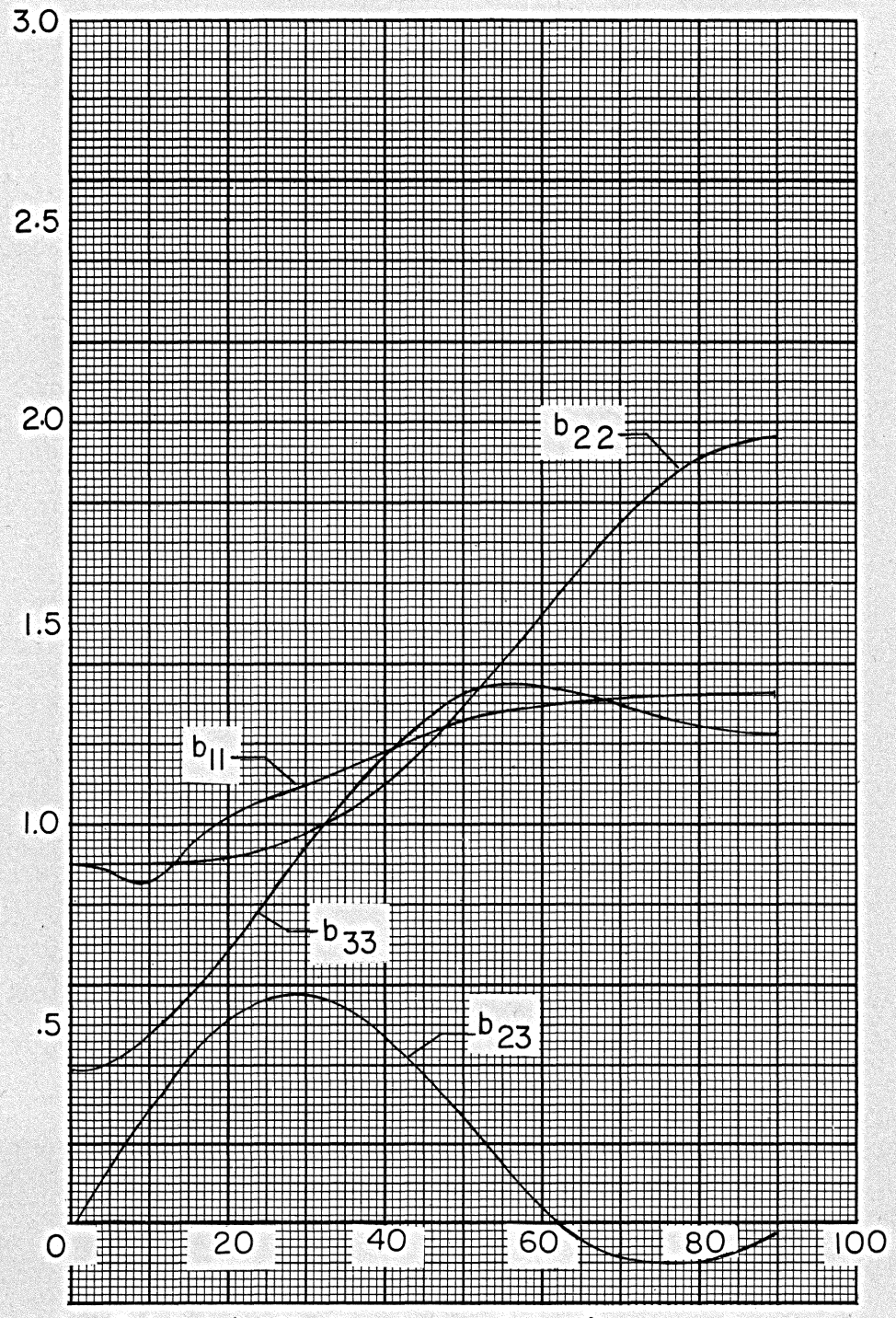

Figure 20.- Elements of B (i_I) matrix as function of i_I
b_{11}, b_{22}, b_{33}, b_{23}.

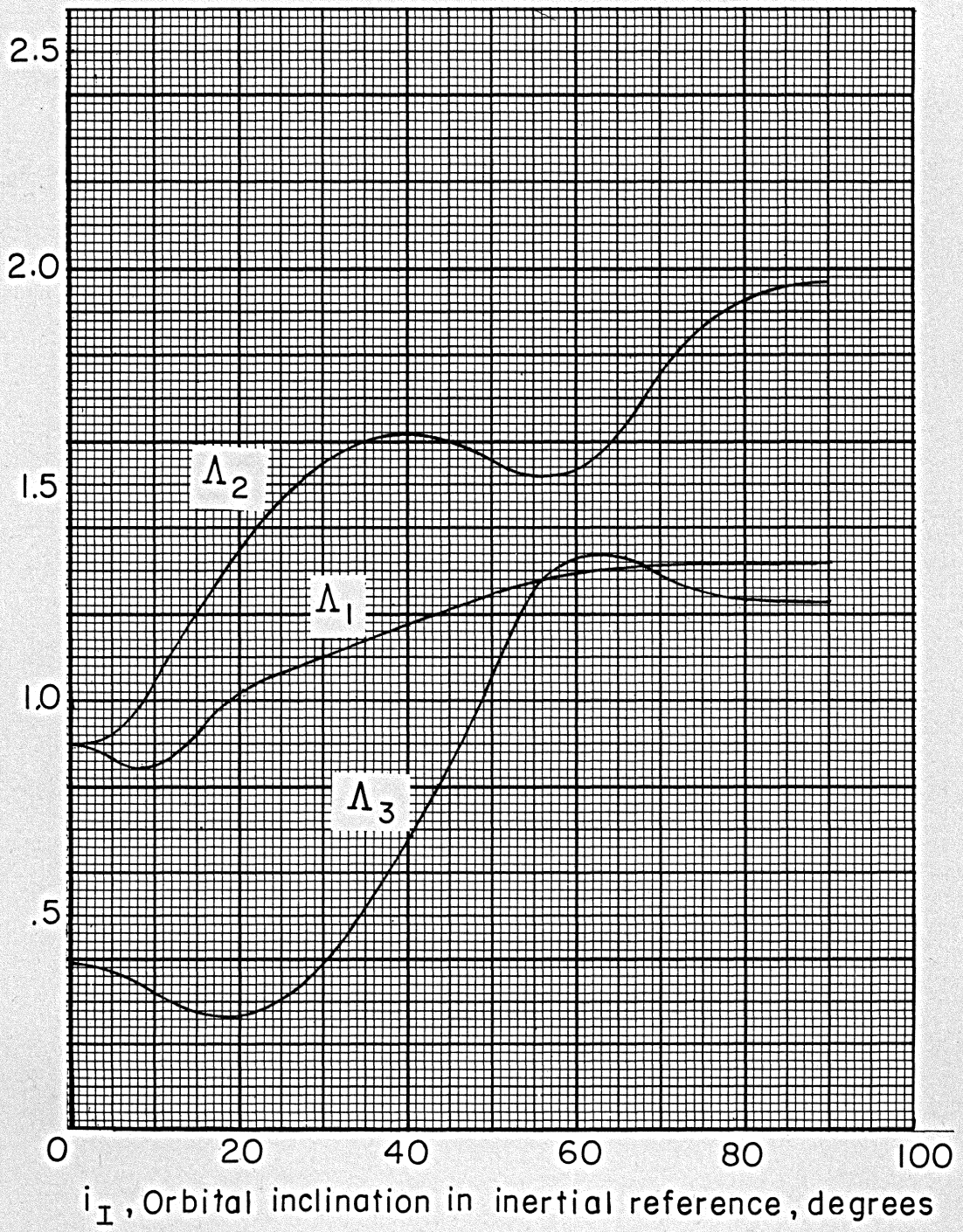

Figure 21.- Eigenvalues of B (i_I) matrix as a function of orbital inclination.

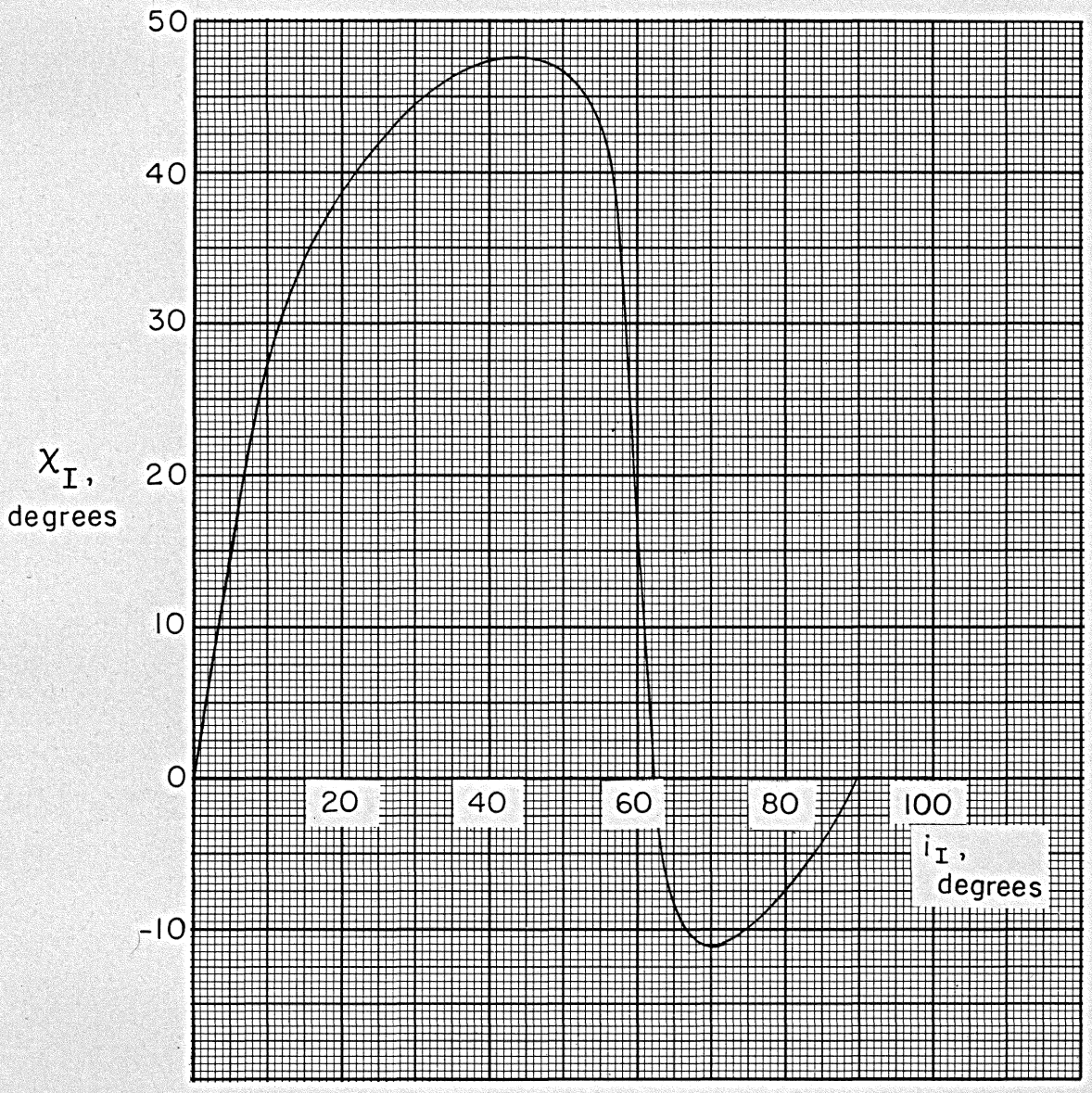

Figure 22.- Angle χ_I, between eigenvectors and coordinate axes, as function of orbital inclination in inertial reference, i_I.

THE TORQUE AND ANGULAR VELOCITY INDUCED BY THE GEOMAGNETIC FIELD ON A SPINNING CONDUCTING SATELLITE

By

G. Louis Smith

ABSTRACT

One source of torque on near-earth satellites is the interaction of the earth's magnetic field with eddy-currents induced in the electrically conducting parts of a spinning satellite. This thesis presents an analysis of this torque, and the resulting spin motions. The analysis consists of two parts: first, the calculation of eddy-current torque due to a given magnetic field, and second, the calculation of this torque and its effect on the angular motions of a satellite.

In the first part, the electromagnetic field equations are applied to spinning and tumbling cylinders, and spinning thin-wall cones, cone frustums, and the general body of revolution. The eddy currents are thus determined for each case, and from this the torque is calculated.

In the second part, the torque which acts on a spinning satellite while in orbit is studied. An expression is derived for the torque vector as a function of the orbit parameters. The time-history of the spin vector subject to this torque is investigated.

Quantitative results of the analysis are presented in graphical form.